8.3.4.4 The dual radiator RICH

Requirements The dual radiator Ring Imaging Cherenkov (dRICH) detector is part of the particle identification system in the forward (ion-side) end-cap of the ePIC detector and complements the forward time-of-flight system and calorimetry, see Figure 8.45. The dRICH has to provide acceptance in the pseudo-rapidity range defined by the ePIC beam pipe and the barrel detector and to operate within the limited envelope allowed by the rest of the compact and hermetic ePIC detector. Distinctive features of the detector are: use of aerogel and gas radiators to extend the covered momentum range, usage of silicon photomultiplier (SiPM) to ensure single photon detection capability in high and not-uniform magnetic field, non-conventional optics with curved active surfaces and compact readout electronics to fit into ePIC.

Requirements from physics: The dRICH is required to provide continuous hadron identification from $\sim$ 3 GeV/c to $\sim$ 50 GeV/c, and to supplement electron and positron identification from a few hundred MeV/c up to about 15 GeV/c. Such an extended momentum range imposes the use of two radiators, gas and aerogel, with a common imaging system to ensure compactness and cost-effectiveness. The radiator gas must ensure π/K separation at 3-σ level up to 50 GeV/c in the most forward region, namely for $\eta > 2$. The aerogel radiator must cover the intermediate momentum interval, bridging the upper limit of the time-of-flight ($\approx$ 2.5 GeV/c) to the Cherenkov threshold of the dRICH gas ($\approx$ 12 GeV/c). These requirements dictate the prescriptions on the refractive index and the radiator chromaticity in the sensitivity region of the photosensors. The dRICH has to provide open acceptance in the ePIC forward pseudo-rapidity range $1.5 \lesssim \eta \lesssim 3.5$. To provide proper light focalization within the due volume, the dRICH active area is located behind the shadow of the barrel detector and its support ring, close to the MARCO solenoid coils. In this region, see Figure 8.46, the $\approx 1T$ strong and not-uniform ePIC magnetic field imposes the use of unprecedented detectors (SiPM).

Requirements from Radiation Hardness: The radiation sensitive components (sensor and front-end electronics) of the dRICH detector are concentrated in a region of moderate radiation level, below O(10^{11}) cm^{-2} n_{eq} of maximum integrated fluence where n_{eq} is a 1-MeV neutron equivalent particle, see Figure 8.47. Close to the beam line, where the integrated dose can reach a value of 15 krad, only radiation tolerant materials reside like silica aerogel [83].

Requirements from Data Rates: The SiPM sensor features an intrinsic significant dark count rate, currently of the order of 50 kHz/mm^2 at room temperature, that indefinitely increases with the radiation damage. To mitigate this effect, the dRICH sensors are operated at low temperature (less than -30°C) and regularly annealed at high temperature (up to 150°C), in order to never exceed a maximum 300 kHz dark rate per channel. The latter value corresponds to a conservative limit taken to preserve the detector performance requirements for Physics and it is supported by present simulation studies that confirm the particle-identification capabilities of dRICH are unaffected.

Justification The specifications outlined above largely define the main technological choices: the momentum range dictates radiator refractive indexes that can be reliably met only by aerogel and gas, while the ePIC environment, space and magnetic field, imposes sensor characteristics that can only be met by SiPM.

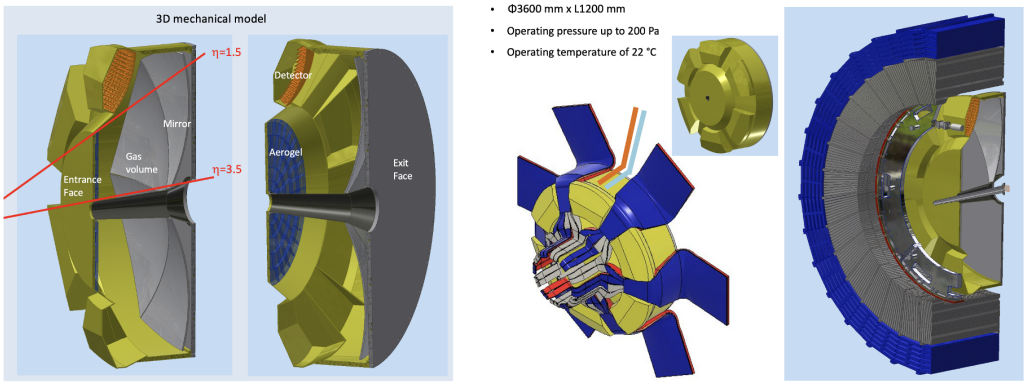

Figure 8.97: (Left) dRICH detector model with highlighted the major components. (Right) dRICH inside the ePIC services lines at the barrel HCAL end point.

Device concept and technological choice: The dRICH is a ring-shaped detector, with a length of 1.27 m and a diameter of 3.6 m, fitting inside the ePIC forward endcap, see Figure 8.97 . The essential components are a layer of aerogel radiator, a volume of gas radiator, and an array of mirrors focalising the Cherenkov light into compact areas instrumented with photo-sensors. The detector is designed in a modular way, with 6 sectors around the beam line of equivalent mirror set and detection area.

The aerogel radiator is a amorphous solid network of SiO_2 nanocrystals whose density regulates the refractive index and chromaticity [3]. The use of silica aerogel for RICH detectors is well established. It is available with refractive indices in the range 1.006–1.08 in between gases and liquids. The current manufacturing methods succeeded in improving the attenuation length Λ (λ = 400 nm) from 20 mm (aerogel used in HERMES) to 50 mm (aerogel for CLAS12 and BELLE-II). The selected aerogel radiator has refractive index n = 1.026 at $\lambda = 400$ nm. The chromatic dispersion has been measured during the R&D phase to be $dn/d\lambda = 6 \cdot 10^{-6}\,\mathrm{nm}^{-1}$ at 400 nm wavelength. Aerogel is typically produced in tiles of few cm thickness: in order to minimize edge effect, the dRICH tile side should be greater than 18 cm, approaching the word record value of 20 cm. The shape and surface flatness of the tiles are important parameters to consider for ensuring optimal PID performance. Typically, due to the fabrication process, aerogel tiles exhibit a slight meniscus shape. Measurements taken during the R&D phase on aerogel samples provided by Aerogel Factory Co. Ltd (Chiba, JP) revealed deviations from the ideal parallelepiped shape by a few tenths of a millimeter, along with a thickness variation between the center and the edges of a similar magnitude. Based on the measurements conducted so far, this deviation from the ideal shape does not impact PID performance. Additionally, the manufacturer has confirmed that improvements in both flatness and thickness uniformity are feasible.

The selected reference gas radiator is hexafluoroethane (C_2F_6), which matches the requirements being characterized by refractive index n = 1.00086 at STP and excellent chromatic dispersion $dn/d\lambda = 0.2 \cdot 10^{-6}\,\mathrm{nm}^{-1}$ at light wavelength $\lambda = 350\,\mathrm{nm}$ [84].

The selected refractive indexes dictates a minimum thickness of 4 cm for the aerogel and O(1) m for the gas in order to ensure enough photon yield. Mirror focalisation is necessary to minimise the consequent uncertainty on the Cherenkov photon emission point. Being inside the detector acceptance, the mirror structure is made of carbon fiber reinforced polymer (CFRP) to ensure the necessary stiffness while being light. In order to preserve the Cherenkov angle information the mirror surface should have excellent optical quality, i.e. few nm roughness and better than 0.2 mrad

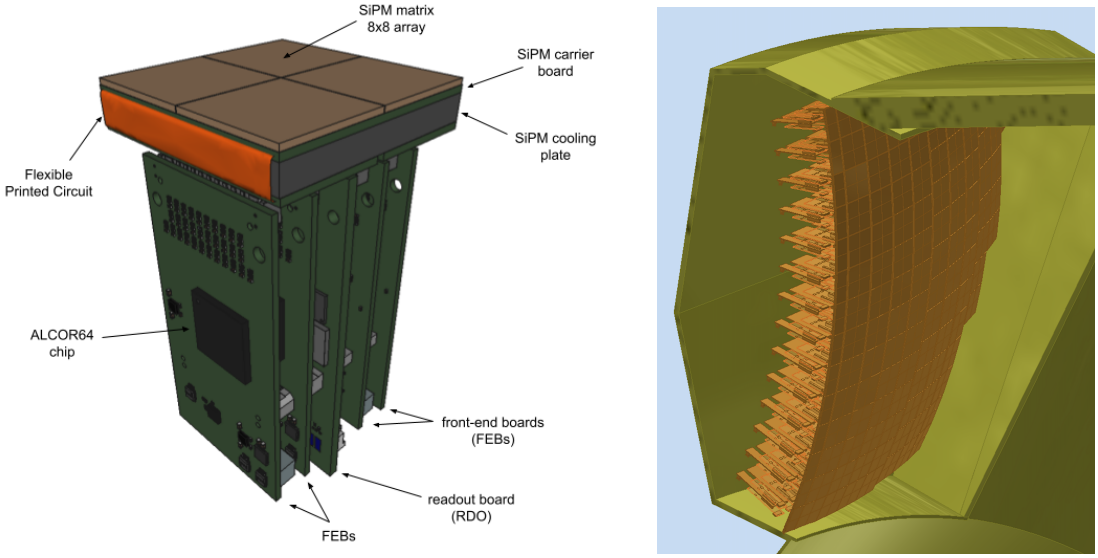

Figure 8.98: (Left) CAD model of the dRICH photodetector unit (PDU) module with its major components highlighted. (Right) dRICH detector box model with 208 PDUs forming a curved active surface.

angular precision (reflecting in a point-like image with more than 90% of the light intensity concentrated in a disk smaller than 2.5 mm). The single mirror dimension is limited to a ≈ 1 m maximum diagonal when accounting for realistic forming mandrel and coating chamber dimensions. In the dRICH mirror array, the radius of curvature should be replicated within 1% of the nominal value and the reflectivity should be better than 90% in the 300-600 nm wavelength range of interest.

The dRICH photon detector surface is shaped over a sphere of radius ~ 110 cm to best approach the 3D focal surface of the mirror array. The Silicon Photomultiplier (SiPM) sensor technology is selected for the photon detector. It ensures superior single-photon counting capability inside the ePIC magnetic field and compact dimensions suitable for tessellating a shaped active surface. The single SiPM sensor has a $3 \times 3\,\mathrm{mm}^2$ area to provide the necessary spatial resolution with an intrinsic time resolution better than 150 ps. The selected front-end ASIC is ALCOR, a 64-channel chip with coupling and rate capability optimized for SiPMs, and a ToT architecture with better than 50 ps LSB [1] resolution in order the SiPM-ALCOR readout chain could achieve an overall time resolution better than 200 ps RMS. To minimize the volume within the dRICH envelope and to maximize the active area, the photodetector is organized in compact photodetector units (PDU). The PDU integrates 256 SiPM channels (grouped into 8×8 arrays in a buttable arrangement to minimize the dead area, which are eventually mounted side-by-side to form a 16×16 array) with the ALCOR TDC readout provided by four front-end boards (FEB), one readout board (RDO) to interface with the ePIC data aquisition (DAQ) and detector control (DCS) systems. In addition, the PDU is designed to allow sub-zero cooling of the SiPMs as well as high-temperature annealing operations. Figure 8.98 (left) shows the conceptual design of the PDU and its main components. The present dimensions of the PDU concept are approximately $52 \times 52 \times 140\ \mathrm{mm}^3$.

Subsystem description:

[1] Least Significant Bit

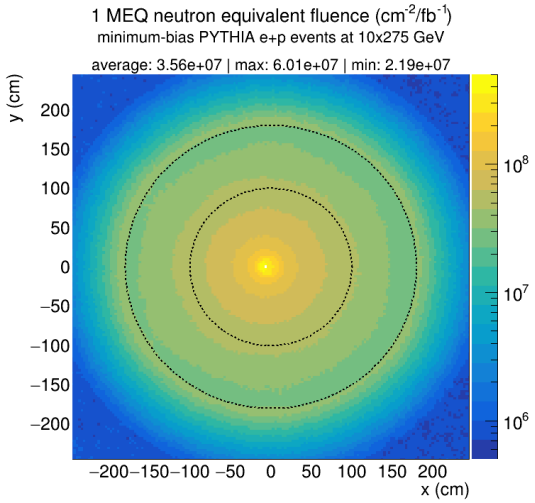

Figure 8.99: Transverse map of the expected 1-MeV equivalent neutron fluence per 1 fb^{-1} of integrated luminosity in e+p interactions at the maximum EIC center-of-mass energy at the location of the dRICH photodetector ($210 < z < 260$ cm). The average, maximum and minimum values within the region of the dRICH photodetector ($100 < R < 180$ cm, indicated by the dashed lines) are reported.

General device description:
Because at ePIC the electron and hadron beam collide at an angle of 25 mrad and aceptance should be provided to the far forward detectors, the common beam pipe cross-section is off-axis at the dRICH location and increasing in area with the distance from IP, imposing an asymmetric layout of the inner components. The aerogel wall is composed of five rings of tiles, each shaped in order to fit inside a 0.2 mm thin aluminum supporting structure. In each sector, focalization is provided by a compound of five mirrors covering a total area of about 2 m^2 with an optimized radius of curvature around 2200 mm. Six independent spherical active surfaces with curvature radius around 1100 mm, each made of 208 PDUs for a total of 53k readout channels, are mounted inside detector-boxes that provide thermal insulation, cooling for the electronics and connections to the services. Given the gas radiator open volume, the Cherenkov photons can be reflected into different detectors depending on the parent charged particle kinematics. The aerogel and photo-detector are separated from the radiator gas by transparent septa, and immersed in a dry (e.g. purged N_2) atmosphere to minimize contaminant absorption and prevent moisture formation. The mirrors are supported by a light carbon fiber structure that is mechanically decoupled from the vessel and allows fine alignment adjustments by means of pizezo-electric motors.

Sensors:
The silicon photomultiplier (SiPM) [85, 86] is chosen as the sensor technology for the dRICH photodetector. The main baseline specifications demand sensors with a 3×3 mm^2 single-channel active area, single photon detection over a broad spectral range from 300 to 900 nm and very high overall photodetection efficiency $> 40\%$ at the peak sensitivity wavelength $400 < \lambda_{peak} < 450$ nm (see Table 8.35 in Additional Material for the full list of the baseline parameters and specifications of the SiPM sensor devices for the dRICH photodetector). SiPMs fulfil the dRICH requirements being cheap and versatile devices with excellent photodetection efficiency (PDE) and time resolution. Their single-photon performance is unaffected by

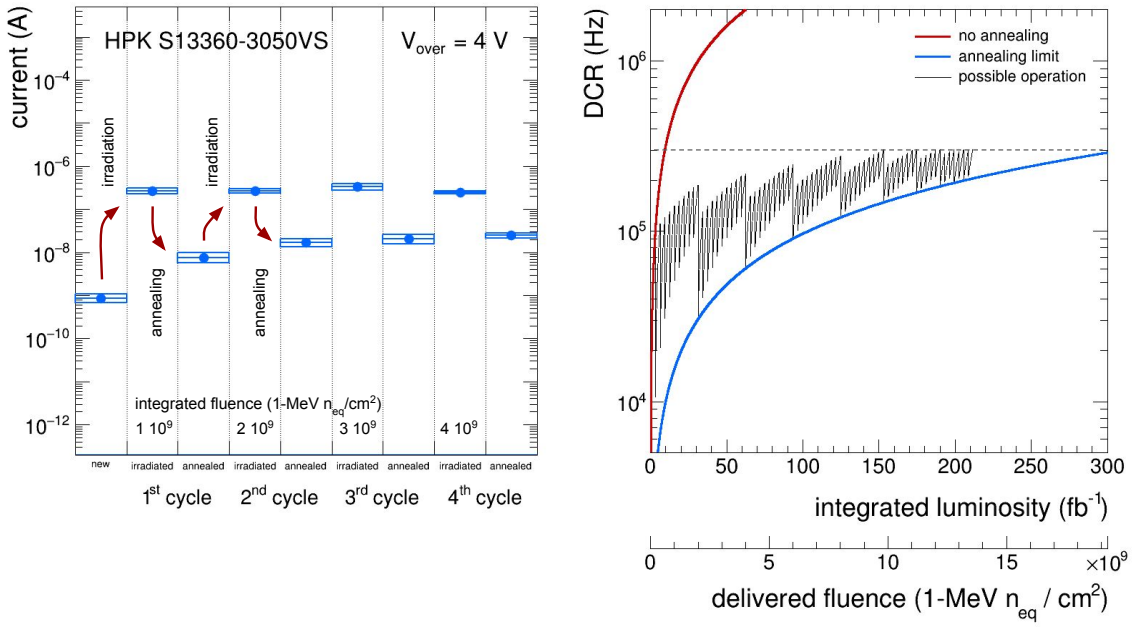

Figure 8.100: (Left) Dark current measurements on sample SiPM sensors for the studies of repeated irradiation-annealing . (Right) Projected increase of the DCR of SiPM as a function of the integrated luminosity (delivered fluence). The "no annealing" and the "annealing limit" curves show the limits of possible operations. The dashed line indicate the desired maximum DCR threshold.

high magnetic fields [**?**, 87], which makes SiPM the only photosensor that can efficiently operate in the field configuration at the dRICH photodetector location in the ePIC experiment, see Figure 8.46. SiPM sensors on the other hand have very high dark count rates (DCR) and are not radiation tolerant. The DCR in SiPM is mostly of thermal origin and it reduces significantly by lowering the SiPM temperature, typically halving every 7-10°C in new sensors [88]. Radiation damage in SiPM is mainly due to displacement damage in silicon, which causes a significant DCR increase and reduces the effectiveness of cooling [89]. At the moderate radiation levels expected at the dRICH location, no significant change in the SiPM parameters (PDE, gain, quenching resistor R_{quench}, pixel capacitance C_{pixel}, breakdown voltage V_{break}) is observed [90]. SiPM cooling is important to keep the DCR low and it becomes crucial after radiation damage [91], as the increase in DCR would be such to make SiPM unusable as single-photon detectors, otherwise. In the dRICH, the SiPMs will be operated at subzero temperature of T = −30°C, or lower. A cooling block is placed in thermal contact with the back-side of the printed-circuit board hosting the SiPMs (carrier board). Cooling fluid in the cooling block will be circulated through a closed loop by a circulating thermostat with dynamic temperature control to regulate and maintain the SiPMs at low temperature. The radiation damage on SiPMs increases moderately with the integrated luminosity. At the location of the dRICH photodetector a maximum (average) fluence of Φ_{eq} = 6.0 (3.6) 10^7 cm^{-2}/fb^{-1} 1-MeV equivalent neutrons (n_{eq} in the following) is expected from e+p interactions at the highest center-of-mass energy of the EIC (see Figure 8.99). Beam-induced background from proton beam-gas events at 35 kHz are expected to contribute bringing the total maximum (average) expected radiation damage to Φ_{eq} = 6.4 (3.7) 10^7 cm^{-2}/fb^{-1} n_{eq}. As shown by the "no annealing" curve in Figure 8.100 (right) and Figure 8.113, the SiPM DCR is expected to

increase with the integrated luminosity at a maximum (average) rate of 31.8 (18.6) kHz/fb^{-1}, reaching a DCR of 300 kHz after an integrated luminosity of approximately 9.5 (16.1) fb^{-1}. These values are based on measurements performed on Hamamatsu S13360-3050 sensors operated at V_{over} = 4 V at T = -30°C, more details are available in Additional Material.

Annealing of SiPMs can be achieved exploiting the Joule effect [**?**]. When a SiPM is forward biased, the microcells composing the device behave as directly polarized diodes connected to their quenching resistors. The current flowing through the resistors eventually heat up the entirety of the sensor. In the dRICH, the circulating thermostat system used for low-temperature operation of the SiPM will be operated in heating mode to warm up the SiPM cooling plate (T = 100°C, or higher) during high-temperature annealing. Therefore a low-viscosity silicone fluid is particularly suitable for cold and heat transfer. Because a fraction of the heating power is delivered by fluid, a reduced current is required to perform the 'forward-bias annealing" to the SiPM. Nonetheless the required power to perform annealing at once over the full dRICH detector is excessively large and unpractical. Therefore annealing operations will be segmented in space and time across the dRICH detector and performed during periods with no Physics beam, and the temperature will be tuned up to T = 150°C, depending on the DCR reduction needs. During the R&D phase it was shown that the "forward-bias mode" approach can cure approximately 97% of the radiation damage. It is therefore expected that a residual irreducible radiation damage (residual DCR) will build up during the dRICH lifetime. As can be see from Figure 8.99 the sensors closer to the beam line will experience a radiation damage almost a factor 3 times larger than those farer from the beam line and will likely require a more frequent annealing. As shown by the "annealing limit" curve in Figure 8.100 (right, maximum fluence) and Figure 8.113 (average fluence), the SiPM residual DCR is expected to increase with the integrated luminosity at a rate of 950 (560) Hz/fb^{-1}, reaching a residual DCR of 300 kHz after an integrated luminosity of approximately 310 (530) fb^{-1}. The "possible operation" curve in Figure 8.100 (right) shows a potential scenario for the DCR evolution for SiPM sensors closer to beam pipe (worst case). This is based on an operation model where more frequent (every $\sim$ 3 fb^{-1}) softer annealing cycles at lower temperature and/or of shorter duration, delivering a DCR reduction of 10 times, are interleave by less frequent (every $\sim$ 30 fb^{-1}) full annealing cycles to reduce DCR as much a possible. A limit in the operation scenario is reached when the annealing is not capable to keep the DCR below the desired threshold or when the annealing frequency become too high. As it can be seen from Figure 8.100 (right), beyond an integrated luminosity of $\sim$ 200 fb^{-1} to keep the DCR below the 300 kHz threshold requires to perform full annealing cycles every $\sim$ 5 fb^{-1}, which is not obviously a practical operation scenario anymore. Some of the SiPM sensors might be needed to be replaced at that stage with new ones or with SiPM sensors of improved performance and radiation hardness as a future upgrade of the dRICH photodetector. One has to keep in mind though that the 300 kHz limit is a conservative value that is connected to the present level of dRICH reconstruction and could be relaxed in future. Moreover, the model shown in Figure 8.100 (right) is based on measurement on Hamamatsu S13360-3050 sensors operated at V_{over} = 4 V in a climatic chamber at T = -30°C. Possible SiPM operation in ePIC at a lower V_{over} of 3 V and at a lower T of -40°C will allow one to achieve lower DCR overall.

FEE:
The ALCOR (A Low Power Chip for Optical Sensor Readout) ASIC, developed by the electronics laboratory of INFN Torino, is the baseline option for the readout of the dRICH SiPM sensors. The architecture of ALCOR and its key specifications are described in Section 8.3.10, here only some specific EIC-driven features are discussed as well as the integration of the ALCOR ASIC into the dRICH front-end electronics. The main goal of ALCOR is to provide single-photon time tagging of the incoming signals, while being able to cope with the SiPMs

inherently high DCR: a maximum DCR value of 300 kHz/ch is expected before an annealing cycle is performed. A good time resolution, better than 200 ps RMS, is required to perform DCR suppression via time gating at both hardware and software levels. A programmable hardware shutter, implemented inside the digital logic of ALCOR, can be enabled to filter out-of-time DCR and provide a significant bandwidth reduction to the system. The time window of interest is controlled off-chip by the RDO FPGA and can be adjusted using in-pixel programmable delays to compensate timing offsets among the 64 channels. With a time window of approximately 2-3 ns, considering that the EIC bunch crossing period is about 10.15 ns, data can be reduced by a factor of 3 or 5. One important point is that the shutter will be needed only when DCR becomes significant due to SiPM integrated radiation damage over time. Therefore, the first period of ePIC data taking can be used to optimize the shutter calibration. The ASIC will be integrated inside a BGA package, providing a compact and robust solution to be assembled on the FEB. A 16×16 mm^2 flip-chip ball grid array (FC-BGA), with 256 balls and 1 mm ball pitch, is the option chosen for the ASIC packaging since it offers more interconnections and better performance w.r.t. standard packaging techniques and matches well with the pixel-matrix geometry of the ALCOR ASIC. A 3D model of the FEB is shown in Figure 8.101. Each FEB hosts one ALCOR BGA device and several components to ensure a stable and safe operation of the system. Linear regulators are employed to provide clean power supplies to the chip and are coupled to I2C interface and current monitors to control the regulators and prevent potential damage from over-current conditions. The FEB incorporates a dedicated PCB section for SiPMs bias voltage routing and also a circuit to enable the SiPM forward-biasing when annealing cycles are carried out. AC-coupling between the SiPM sensors and ALCOR inputs has been chosen to isolate them when the SiPMs are operated in forward bias.

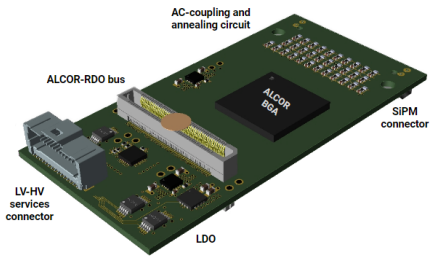

Figure 8.101: 3D model of the dRICH FEB.

Other components:
The radiator gas in the RICH vessel is controlled by the gas radiator system, see Figure 8.102. Its main tasks are, during detector operation, (i) providing well controlled pressure conditions in the 12 m^3 RICH vessel to avoid relevant pressure difference at the vessel walls and at the fused silica windows; (ii) removing oxygen and water vapor contaminates, in order to prevent building up impurities due to air leaks entering the gas system; (iii) performing detector vessel filling with hexafluoroethane before a data taking period and radiator gas recovery at the end of the period; the filling/recovery is from/to the storage tank. The main components of the radiator gas system are two oil-free compressors, working in parallel, which continuously extract gas from the vessel at constant rate in order to ensure the gas circulation, a pressure sensor installed on top of the radiator vessel for continuous monitoring of the internal relative pressure and to dictate the opening level of a flow control valve on the input line, adjusting the opening so to preserve the relative pressure inside the vessel. Oxygen and water vapor traces are removed by filtering cartridges with molecular sieves and Cu-catalyst, which are permanently in series in the circulation system, to maintain a

contamination level better than 20 ppm (a value less stringent than for gas devices working in the VUV wavelength region). The gas temperature and pressure will be continuously monitored to correct the variation of the refractive index within an uncertainty below 0.1% in terms of (n-1). The vessel is flushed with nitrogen during the shutdown periods. Nitrogen and hexafluoroethane separation during filling and recovery is under study and two options can be envisaged: (i) the use of osmosis via dedicated membranes or (ii) via a two-step procedure: replacing nitrogen with carbon dioxide and then performing distillation at $-35°C$. Hexafluoroethane is a greenhouse gas and, therefore, the residual C_2F_6 present in the nitrogen/carbon dioxide cannot be vent out: it must be collected and trapped for disposal with a dedicated recovery system. The control of the whole radiator gas system is performed via a Programmable Logic Controller (PLC). More details are provided in Additional Material of 8.3.4.4.

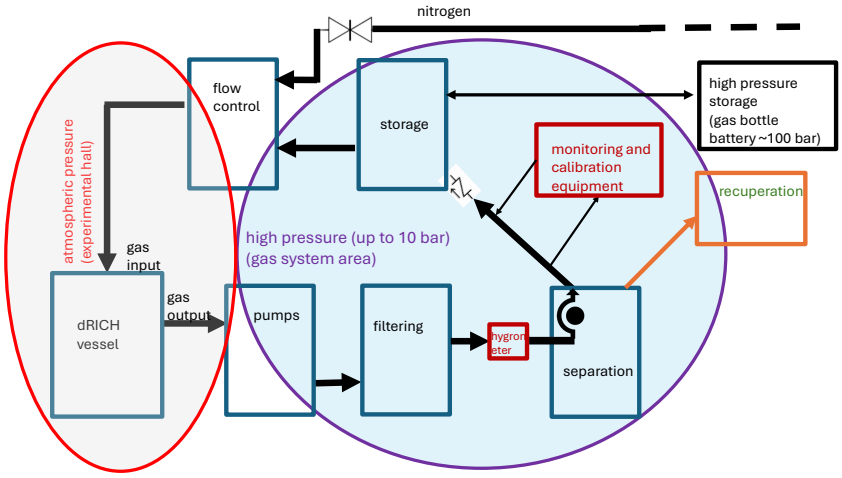

Figure 8.102: Block diagram of the dRICH gas system.

Performance

For each recorded dRICH hit, the photon path is reconstructed taking into account the charged particle trajectory and the focalising optics of the detector, in order to provide an estimate of the Cherenkov angle at the emission point. The combined information of all the Cherenkov photons associated to a charged particle result in a precise determination of its velocity βc and, knowing the momentum from the ePIC spectrometer, its mass. The dRICH model is part of the ePIC simulation framework and allows complete performance studies taking into account quality of the track reconstruction, bent trajectories (by magnetic field) and multiple scattering. To bypass the complexity of such a framework, some specific study can be anyway performed with private or simplified simulation chains. The laboratory characterization and the numerous test-beams have provided detailed inputs for modeling in a realistic way the single components and global detector response. In the dRICH, the contributions to the single-photon (SPE) angular resolution have a different weight depending on the radiator. The dRICH has been designed in order to keep most of the contributions to the SPE angle resolution close or below 0.5 mrad, see Figure 8.103, a value dictated by the tiny Cherenkov angle difference between pions and kaons at 50 GeV/c in the radiator gas. The single SiPM readout channel has been limited to 3×3 mm^2 area. The MARCO coils and the dRICH position has been optimized in order to minimize the bending inside the radiator gas volume. The tracking resolution is assumed to cope with the same constrain. Note that combining

N photons the angular precision scale with a maximum $N^{-1/2}$ factor only in case of a completely uncorrelated information, a condition that is not valid for the bending and tracking contributions. The uncertainty on the emission point is not an issue for a few cm layer of aerogel, but is critical for a 1 m long gas volume, expecially within the limited space available in ePIC for the optics: this remains the major contribution to the SPE resolution of the radiator gas despite the mirror focalization and the curved dRICH detector surface. Because the present model assumes a single radius for the dRICH mirros, optimized for the forward rapidity region to boost the high-momentum reach, the resolution worsens with the polar angle increase. This is not a problem, because the average particle momentum decrease as well loosing the performance requirement. The chromatic error is well under control for gas but is the largest contribution to the angular resolution for the aerogel. This derives from the intrinsic nature of the radiator in conjunction with the quantum efficiency characteristic of the photosensor. The chromatic uncertainty limits the aerogel momentum reach to something above 15 GeV/c, a value well above the Cherenkov threshold of kaons in gas, high enough to provide the wanted overlap between the measured ranges of the two radiators.

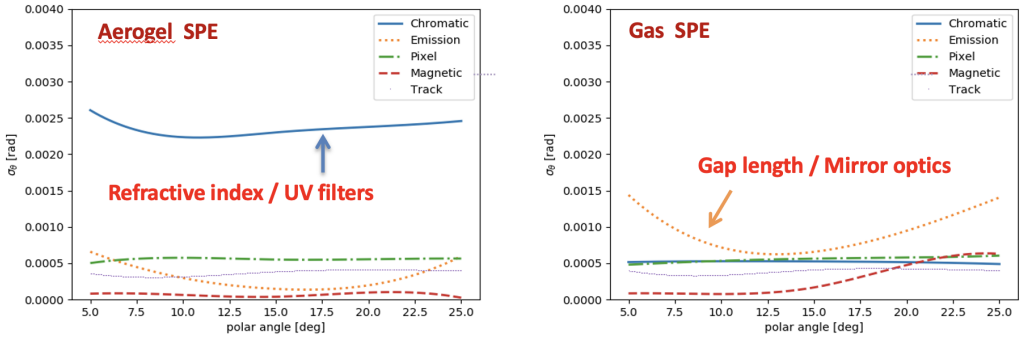

Figure 8.103: (Left) Contributions to the single-photon angular resolution for aerogel. (Right) Contributions to the single-photon angular resolution for radiator gas.

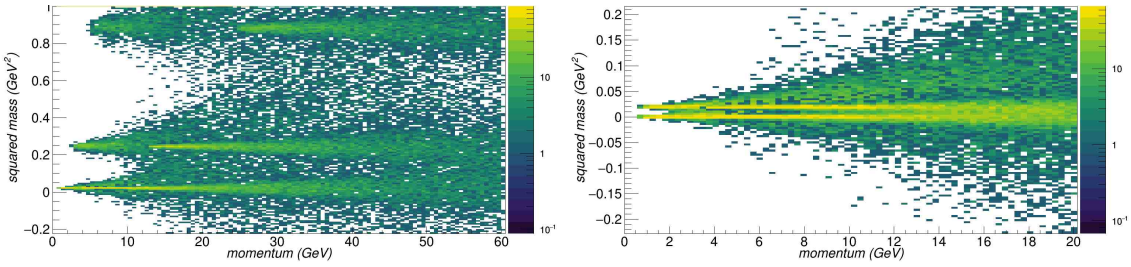

Figure 8.104: (Left) Reconstructed mass vs momentum for pions, kaons and protons. (Right) Reconstructed mass vs momentum for pions and electrons. Distinct values derived from aerogel and gas are shown, to highlight the complementary coverage and effective interplay of the two radiators. The study is performed at the large rapidity endpoint $3.2 < \eta < 3.5$.

The number of emitted photons varies with the pseudo-rapidity due to the different path of the particle within the radiators. The mean number of recorded photons is about 18 for the radiator gas and 12 for the aerogel for a particle with momentum well above the Cherenkov threshold. In average, few charged particles per event are expected to hit the detector. With a proper pattern recognition and photon path reconstruction, the information of the two radiators can be combined to extend the hadron momentum coverage of ePIC PID from the TOF $\approx$ 2.5 GeV/c upper momentum limit to above 50 GeV/c, and support electron separation up to 15 GeV/c, see Figure 8.104. In

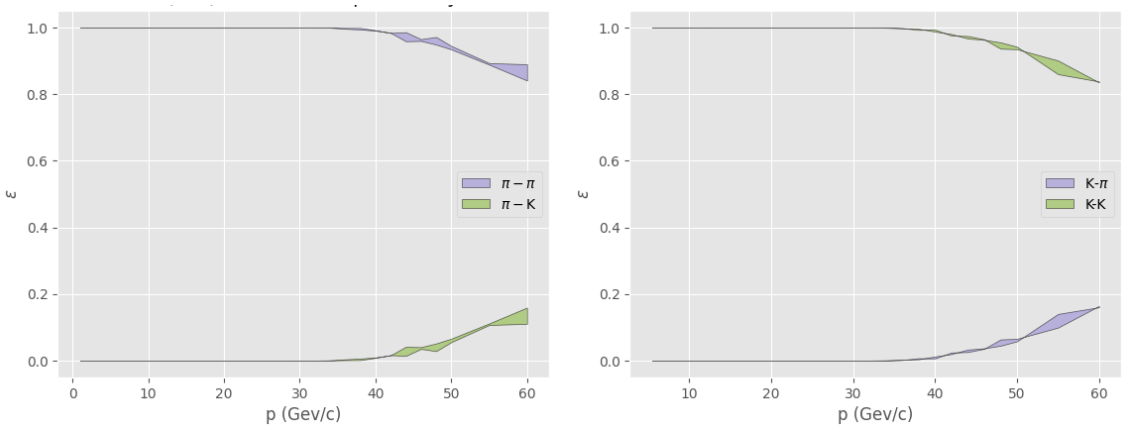

Figure 8.105: (Left) Pion identification efficiency and pion to kaon mis-identification probability as a function of momentum. (Right) Kaon identification efficiency and kaon to pion mis-identification probability as a function of momentum. Both estimates are made at the large rapidity endpoint $3.2 < \eta < 3.5$.

.

the forward direction with optimized focalization, an identification efficiency greater than 95 % at a corresponding 5 % percent mis-identification probability, is achieved, see Figure 8.105. As expected from the resolution study, the momentum reach is reduced with the pseudo-rapidity, in accordance with the kinematics of the particles expected from physics reactions, see Figure 8.122.

Implementation

Services:

The dRICH services are grouped into power lines for sensors, electronics and slow control monitors, gas lines for the radiator gas volume, the aerogel inert gas volume, and cooling lines for the sensors and electronics. Table 8.31 shows a list of the power services for the dRICH photodetector. Eighteen 19" wide/8U mainframes (approximately $50 \times 40 \times 70$ cm^2 each) capable to host 16 boards each are needed to accommodate the low-voltage and high-voltage boards. The primary power-supply channels will serve multiple modules at the same time, with a typical grouping of 1024 SiPM channels. Nonetheless, further segmentation is implemented on the detector electron-

Name	Voltage (V)	Current (A)	Channels	Boards	AWG gauge
Analog	1.4	10.0	312	39	10
Digital low	1.4	8.5	312	39	11
Digital high	2.7	6.0	312	39	12
Master panel	5.0	5.2	6	1	13
SiPM bias	64.0	1.3	12	2	19
Annealing	12.0	3.2	1248	156	15

Table 8.31: List of the voltage services to the dRICH electronics, indicating the number of primary power-supply channels and boards as well as the cross-section of the cables (AWG). The number of power-supply boards is defined assuming to use commercial 8-channel low-voltage boards.

ics, reaching a low-voltage power segmentation of 64 SiPM channels and a high-voltage power segmentation of 32 SiPM channels. The circulating thermostat system should be capable of circulating approximately 50 l/min of fluid at a maximum pressure of 1.5 bar in a broad temperature range (from -60°C to 120°C). Possible commercial systems are available, but more time is needed to better investigate the options. It is expected that a potential circulating thermostat system with the desired characteristics will require space in the experimental hall for a volume of approximately $1.3 \times 0.8 \times 1.6$ m^3. Manifolds are needed to split the fluid from the thermostat into 6 loops, each feeding one dRICH photodetector box. A solution without manifold and 6 smaller independent thermostat unit for each dRICH sector will be investigated as a possible optimization. Insulated pipes will be needed to transport the fluid from the thermostat to the detector, and back. The insulation must guarantee no frost and no water condensation on the pipes when operating at the lowest temperatures and is also required to limit transport losses in heating/cooling capacity. Cooling for the front-end electronics is required to remove the approximately 15 kW of heat generated by the dRICH photodetector ($\approx$ 2.5 kW in each of the six photodetector boxes). Force-air circulation in the boxes with diffusers are being studied as a possible effective solution. It is important that the air-cooling system for the FEE electronics provides dry air with a dew point well below the SiPM operating temperature. A system based on forced circulation of gaseous nitrogen might be well suited also to ensure an inert environment inside the detector boxes. Gaseous nitrogen will be used to maintain the aerogel in a clean and inert environment. The radiator gas system and its related monitoring equipment require a surface of about 15 m^2, in order to host 5 racks of instrumentation, the gas storage tank and a support for the spectrophotometer. This surface includes the space needed by the operators. Various sections of the gas system operate at a 2-3 bar pressure, while the cell to measure and monitor the gas transparency operates at 10 bar. Some gas bottles at typical high pressure (100-150 bar), organized in a battery, have to be included to provide the radiator gas at filling and house it when recovered. The pipelines connecting the gas system to the vessel are 70 m long with a diameter of 10 cm.

Subsystem mechanics and integration:
The dRICH structure can be described by two disks, one entrance window of 0.9 m radius supporting the aerogel radiator and one exit window of 1.8 m radius mounting the mirror system, connected by two ring-shaped structures, an outer shell that mounts the six detector boxes and one inner pipe surrounding the ePIC beam pipe. All the elements are made in composite materials. The pipe and shell are made by a carbon fiber reinforced polymer (CFRP) bulk to provide support strenght. The two windows are a sandwich of two thin carbon fiber skins and a core honeycomb to limit the material budget to about 1% of radiation length each. The shell and detector boxes are shaped in order to allow the passage of all the services of the inner barrel detectors, see left panel of Figure 8.106. The dRICH services are concentrated on the shadow of the detector boxes and do not interfere with the routing of the others. A dedicated scaffolding would be realized to allow the installation of the detector, and the roll-in and roll-out movements to the service position without interference with the beam pipe to preserve the beam vacuum, see central and right panel of Figure 8.106. The dRICH is suspended inside ePIC via brakets connected to the HCAL barrel.

Calibration, alignment and monitoring:
Dark counts in SiPMs are indistinguishable from photon-induced signals and owing to the large SiPM DCR there is no need of a dedicated system to evaluate the functioning of any given readout channel. A measurements of the DCR as a function of the front-end electronics discrimination threshold can provide information on the signal amplitude. Using solely the dRICH readout system it is therefore possible to measure the signal amplitude as a function of the bias voltage, hence to obtain information on sensor functioning, breakdown voltage and gain at different operation

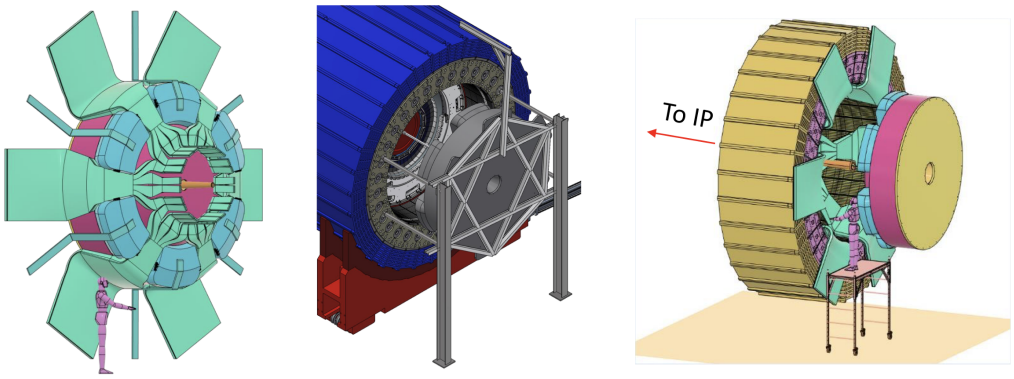

Figure 8.106: (Left) Service routing around the dRICH. (Center) Installation tool. (Right) Maintenance position.

conditions. Timing calibration of the SiPM sensors can be achieved with a picosecond pulsed laser light system. The light from the laser is brought inside the dRICH volume via optical fibres. The light from the laser directly impinges on a diffuser that eventually illuminates the full area of one dRICH photodetector sector. At least one laser-fibre-diffuser system is needed for each dRICH sector. The time delay due to the different path of photons from the diffuser to the SiPM that detects the light is known and can be corrected to achieve a relative calibration of the times of SiPMs within the same sector. Absolute timing calibration can then be achieved with collision data. Sample particles from physics reactions can be used to perform fine adjustment of the calibration costants. Electron particles identified by other ePIC subsystems can be used to correct residual misalignment or calibrate the radiator refractive index thanks to the saturated Cherenkov rings. Known particles from meson decays (Λ, ϕ, K_S, ...) identified by kinematics criteria can be used to verify the parameters of the dRICH reconstruction and the consequent PID performance. The calibration and monitoring equipment of the radiator gas and gas system (see Additional Material of 8.3.4.4) includes a set of temperature sensors placed inside the dRICH vessel and equipment on-line in the gas circulation loop. A commercial hygrometer and a commercial oximeter, a transparency measurement system by a commercial spectrophotometer equipped with a high pressure ($\approx$ 10 bar) cell and a Jamin interferometer setup complete the set of the equipment. The interferometer, complemented with temperature and pressure sensors, will provide in real-time the refractive index of the gas in the vessel. The refractive index measurement has a twofold role: during filling/recovery, it monitors the hexafluoroethane level in the vessel, during operation it will provide in real time the refractive index of the radiator gas to make possible quasi on-line data reconstruction as foreseen in the ePIC streaming read-out model.

Status and remaining design effort:

R&D effort:

SiPM sensors. A station has been realized to characterize the SiPM sensors inside a climate chamber to control the working temperature, see left panel of Figure 8.107. The readout chain is based on ALCOR to reproduce the ePIC configuration. Such a station allowed detailed performance comparison between SiPMs of different manufacturers and types, see Figure 8.107 (central panel), and different ageing due to radiation and annealing. The R&D results on photosensors reported here are those obtained with Hamamatsu S13360-3050 sensors operated at V_{over} = 4 V in a climatic chamber at T = -30°C, unless otherwised specified. Nonetheless, the qualitative features of the results are valid also for other types of sensors.

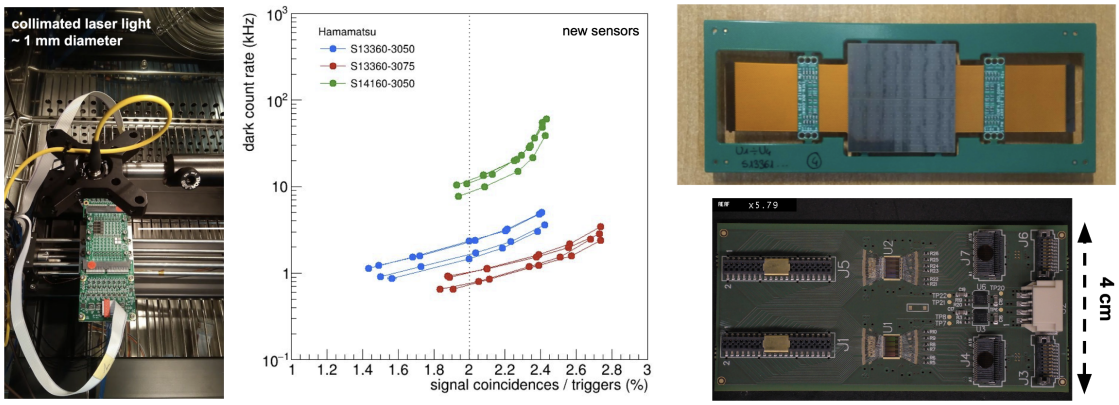

Figure 8.107: (Left) Test stand for SIPM characterization. (Center) Performance comparison between different SiPM models. (Right) Prototype version of the SiPM carrier board (top) and FEB (bottom).

Irradiation tests performed to simulate a realistic experimental situation where SiPMs experience repeated irradiation and annealing cycles (see left panel of Figure 8.100) show that each irradiation cycle produces a consistent DCR increase (approximately 500 kHz for a 10^9 cm^{-2} n_{eq} irradiation) and a consistent residual DCR (approximately 15 kHz for a 10^9 cm^{-2} n_{eq} irradiation) remains after an annealing cycle in a thermostatic chamber. The fraction of damage cured by such a "oven annealing" cycle is of approximately 97% of each newly-produced irradiation damage. The residual damage builds up after each irradiation-annealing cycle and seems to be irreducible within the details of this annealing protocol. Irradiation tests and laboratory measurements show that the "forward-bias annealing" mode can cure radiation-induced damage on SiPM (see left panel of Figure 8.108) to the same effectiveness level as the one measured for the "oven annealing" with a residual damage of approximately 3%. The benefit of the "forward-bias annealing" is significant: an extended SiPM sensors lifetime that can be achieved over the delivered radiation damage without the need to directly access the detectors in the experimental cavern. Higher temperatures and longer annealing times lead to more effective annealing. On the other hand, a limit seems to be reached already at T = 150°C as annealing at a higher temperature like T = 175°C does not lead to improved current reduction. Laboratory measurements performed so far show that the temperature of the SiPM increases with respect to the temperature of the SiPM carrier board proportionally to the power delivered by the forward-bias current. Figure 8.108 (right panel) shows that, as expected, the increase of SiPM temperature linearly depends on the annealing power and it is the same at different values of circulating thermostat temperature. It is therefore sufficient to monitor the temperature of the SiPM carrier board and deliver the needed annealing power to have control of the SiPM temperature and keep the process safely under control. Laboratory measurements reported here are performed in an open environment at room temperature. With the circulating thermostat temperature set at T = 100°C, a SiPM annealing temperature of T = 150°C is reached with approximately a power of 0.5 W/sensor, which corresponds to a forward-bias current of approximately 60 mA/sensor. With the SiPM placed in a closed environment as the dRICH photodetector box, one would expect a lower power needed that will be measured during detector construction. Laboratory measurements show that for annealing temperatures up to T = 150°C there is no significant degradation of the PDE up to annealing times of 150 hours. More studies will be done, but at the time of writing annealing at T = 150°C can be considered safe for the expected dRICH operations.

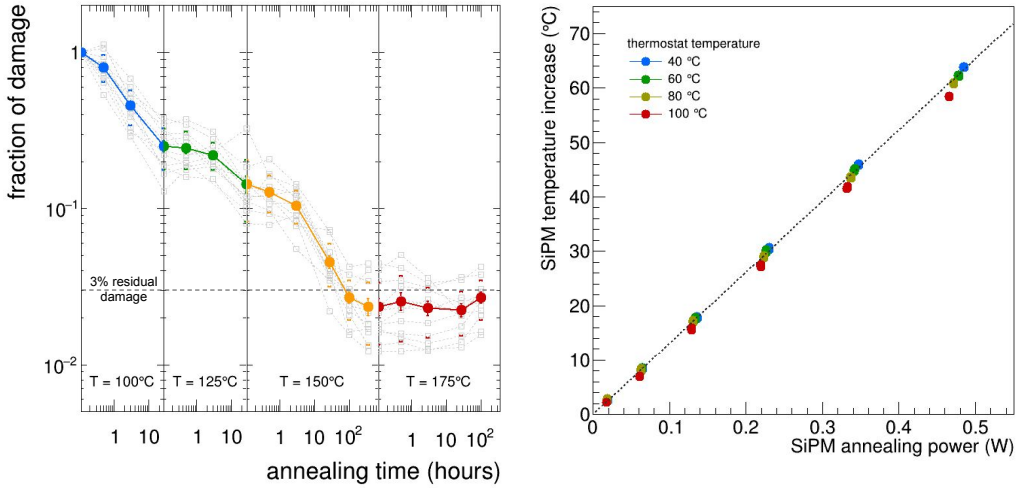

Figure 8.108: (Left) Fraction of residual irradiation damage measured on multiple SiPM candidate samples after "forward-bias annealing" cycles at increasing temperature and integrated annealing time. The measurements are shown for individual sensors (gray points) and as averages (coloured points, uncertainty of the average and RMS are indicated on the plot). (Right) Temperature increase of the SiPM sensor with respect to the temperature of the SiPM carrier board as a function of the "forward-bias annealing" power at different temperature values of the circulating thermostat system.

FE Electronics. ALCOR has been extensively used within the ePIC dRICH Collaboration since 2021, testing it coupled to different SiPM models and assessing its single-photon time-tagging capability and time resolution. A prototype version of the SiPM carrier and FEB board have been developed, see right panel of Figure 8.107. The SiPM carrier provides electrical connections via thin kapton cables in order to bypass the sensor cooling plate. The prototype FEB hosts two 32-channel ALCOR chips which are directly wire-bonded on the PCB. It has been designed using specifications close to the ones for the final FEB, i.e. having the same dimensions and incorporating the same number of channels (64). It is served by a master-logic board that provide bias control and temperature monitor. These boards have been extensively used for the 2023-2024 dRICH activities, including two successful beam tests. ALCOR has been tested for radiation hardness with results showing only some small degradation on the TDC performance after a total ionizing dose (TID) of 300 krad, which is O(100) times the expected TID in ePIC. The single-event upset (SEU) cross section has been measured to be $3.3{\cdot}10^{-15}$ cm^2/bit, which corresponds to an expected mean time between failure due to SEU of about 190 hours for the entire dRICH detector. These results confirm that the technology is sufficiently radiation tolerant to be used in the ePIC dRICH environment.

Radiator gas. The transparency in the near-UV benchmark region (most sensitive to the gas quality and contaminants) has been measured with a monochromator at CERN, resulting in values above 98% for a 1.6 m coloumn of gas at wavelengths grater than 200 nm, see left panel of Figure 8.109. The measurement has been done with a gas that was stored into bottles for about 4 years, indicating an excellent preservation with time.

Aerogel. The transparency of several aerogel samples has been measured using a spectrophotometer at CERN and at INFN. Aerogel tiles with different refractive index (n = 1.015-1.026, 1.03, 1.04, 1.05) and 2 cm in thickness have been tested. At the wavelenght of 400 nm,

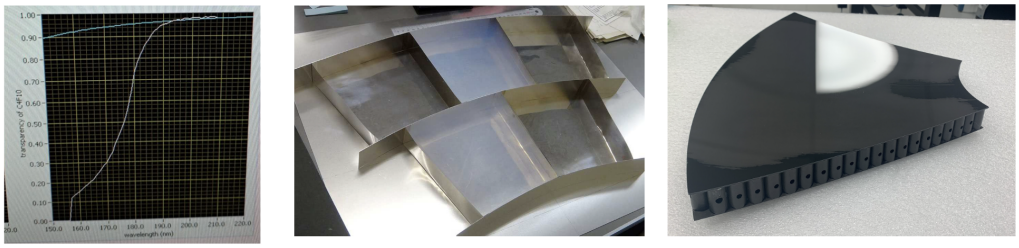

Figure 8.109: (Left) C_2F_6 measured transmittance in the near UV-region. (Center) Aerogel large tiles assembling as obtained at BELLE-II [3]. (Right) Mirror demonstrator with an optimized dRICH core structure.

the transparency vales are pretty good and typically above 70 %. The tiles with n = 1.03 show the highest values. In general the tiles have the shape of a dome as a consequence of the production process. In the metrology laboratory at CERN, the thickness and flatness of the tile have been also measured. The measurement has been executed on a tile with $n = 1.03$ using the touch probe system (force applied = 2 g). The measuring system is the LEITZ PMMC with $\pm$ 0.3 μm of precision. There is a variation in thickness from the center to the edges, of the order of 0.4 mm, and a different planarity in the two faces, one 0.7 mm, the other 1.27 mm. These values are unexceptional but are not a reason of concern.

Mirror. A mid-size demonstrator (of 60 cm diagonal) has been realized with dRICH specifications, see right panel of Figure 8.109. The CFRP core structure has been optimized for preserving the surface shape accuracy and a light body: it adopts the light LHCb structure in the center, and the stronger CLAS12 structure on the edges. Before coating, the point-like source image test measures a D0 value, that represents a global surface quality estimator, of 1.8 mm, better than the specification of 2.5 mm. The same test indicates a radius of 2254 $\pm$ 5 mm, slight above the request to be within 1% of the nominal 2200 mm value.

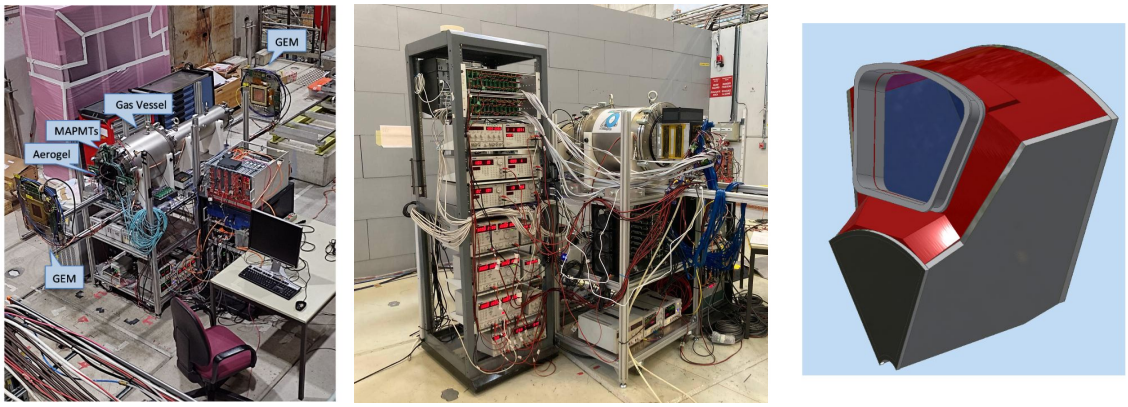

Figure 8.110: (Left) Baseline prototype with reference multi-anode PMT sensors at the SPS-H8 beam line of CERN. (Center) First ePIC-drive SiPM detector box under test at the PS-T10 beam line of CERN. (Right) Real-scale prototype model mimicking the basic dRICH construction unit (sector).

Prototyping. A baseline prototype has evolved in time to serve the dRICH R&D development for few years, see left panel of Figure 8.110. The gas vessel is a cylinder made of vacuum standards, to allow an efficient and safe gas exchange. The entrance flange can mount

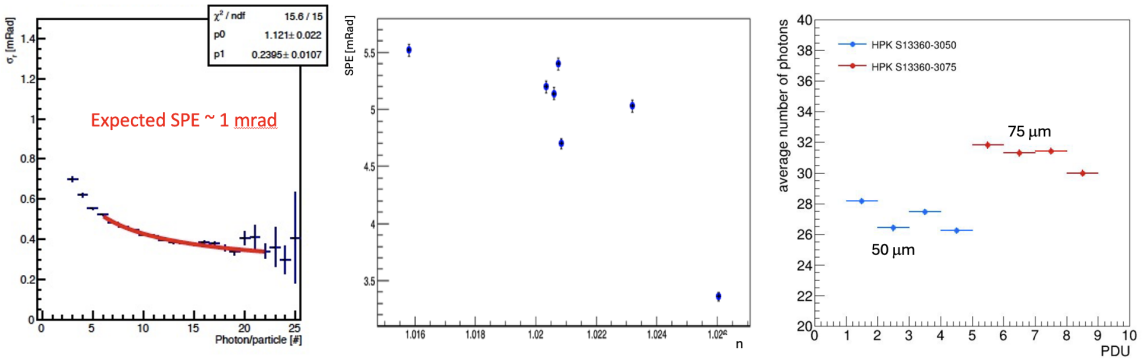

Figure 8.111: (Left) Cherenkov angular resolution obtained for C_2F_6 as a function of the recorded number of photons. The SPE values is consistent with expectations. (Center) SPE angular resolution measured on aerogel as a function of the refractive index. The expected resolution is obtained for an index greater than n=1.025. (Right) Comparison in photon yield of sensor with different SPAD size. All the measurements has been obtained with the dRICH prototype.

an external dark box separated from the inner gas volume by a UV-transparent lucite foil (or quartz window). An aerogel tile with possible additional UV filters, plus an array of alternative sensors and readout electronics, can be inserted into the dark box. Two mirrors inside the vessel have optimized focal lenghts to image the Cherenkov light from the two radiators onto the limited active surface. The major achievements obtained during several test-beams have been the validation of the dual-radiator concept, the validation of the C_2F_6 gas radiator (see left panel of Figure 8.111), the optimization of the aerogel refractive index (see central panel of Figure 8.111), the performance study of the SiPM-ALCOR readout chain (see right panel of Figure 8.111), and the development of an EIC-driven readout plane. A partially equipped EIC-driven plane has been realized in time for the October '23 test-beam with Hamamatsu S13360-3050 SiPM sensors of standard 50 μm pixel pitch, see left panel of Figure 8.112. The plane has been complemented for the test-beam in May 2024 with sensors of 75 μm pixel pitch, to verify the potential benefit in timing and photon detection efficiency. This has allowed for the first time a full ring coverage, an essential requirement for precise radiator performance study and effective signal over background study, see central panel of Figure 8.112. An effective interplay between the two radiators at intermediate energies has been demonstrated, see right panel of Figure 8.112. The new detector box has allowed a preliminary study of the thermal gradients and possible effects on the gas performance, indicating that the possible temperature gradient of few degrees induced into the gas volume by the cool sensor plane can be largely mitigated by a gas re-circulation or by a double window.

E&D status and outlook: The study of SiPM performance continues with irradiation cycles of different particle type and more and more optimized annealing protocols to achieve the best PDE and time resolution preservation. A new version of the ALCOR ASIC is currently being designed to extend the number of channels to 64 and integrate the chip inside a BGA package (FC-BGA technology with 256 balls and 1 mm ball pitch), aiming to enhance the scalability of the readout system and meet specific EIC-driven requirements. The new version of ALCOR will also include some internal design revisions. These include a programmable hardware shutter to filter out-of-time DCR and thus significantly reduce the data throughput, an increased bandwidth amplifier to improve the system time resolution while keeping the same power consumption and an hysteresis circuit in the discriminator stage to avoid unwanted re-triggering on the SiPM signals slow tail, occurring when operating with

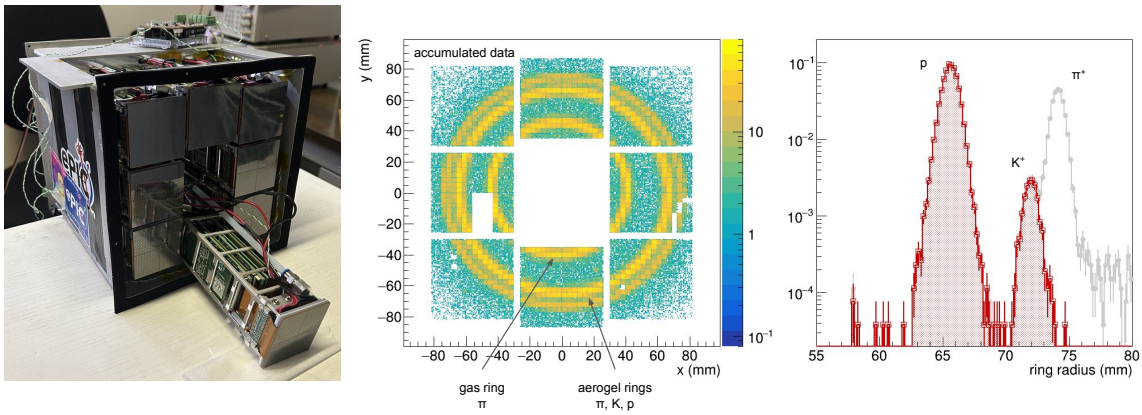

Figure 8.112: (Left) Prototype PDU and assembled detector plane. (Center) Cumulated ring imaging. (Right) dual-radiator interplay for a mixed hadron beam at 10 GeV/c: After the gas information is used to tag pions (clear histogram), an effective separation between kaon an proton is provided by the aerogel (shaded histogram).

very low thresholds. The tape-out is scheduled during the first months of 2025. A thorough electrical characterization of this version of ALCOR, the first one assembled in a BGA package and including all the features required for the dRICH application, will be carried out to validate its new functionalities and measure its performance in order to complete the E&D activity and go ahead with the ASIC mass production which is foreseen in 2026. The development of the final front-end boards takes advantage of the work done for the prototype version in terms of space constraints, readout scheme and components selection. The design of the final version of the SiPM carrier, FEB and master-logic boards will be completed in 2025 while the mass production is expected during 2026. For the radiator gas, it is required to complete the design of the gas system and finalize the layout of the monitoring equipment. A dedicated system will be developed to measure the gas transparency in the visible wavelength range. Each of these activities assumes an engineering study and its validation by laboratory studies. The remaining E&D activity is expected to be completed by the end of 2026. An increase of the aerogel tile volume is instrumental to minimize the edge effects and contain the cost. During the R&D phase, tiles with side up to 15 cm and thickness up to 2 cm were realized. A feasibility study is ongoing to increase these limits towards a side of 20 cm or a thickness of 3 cm to support the successful assembling scheme adopted at BELLE-II, see central panel of Figure 8.109. The aerogel production efficiency should be evaluated in conjunction with the optical quality and precise shaping obtained. This engineering work is expected to take time and not be completed before the end of 2026. Coating of the CFRP mirror substrate should be realized and compare with the benchmark performance obtained with the similar materials at CLAS12. This work will be completed by mid 2025. A real-scale prototype is being realized with composite materials and a realistic geometry (mimicking a dRICH sector). This is instrumental to validate the mechanical elements and study the assembling details (e.g. of transparent septa), the mechanical stability, the gas tightness, and the thermal aspects. One of the major goals of the real-scale prototype is also to reproduce the final ePIC working conditions, mount an extended readout plane with the designed RDO board, operate demonstrators of the optical components as results of the ongoing developments, and optimize the performance in a realistic off-axis optics configuration. To this end, a test-beam is planned for mid 2025.

Other activity needed for the design completion:

Slow control, interlock and the calibration LED/laser system design is not started yet.

Status of maturity of the subsystem:
The R&D activity has been focused on the most innovative aspects of the detector that present technological challenges. These are the SiPM for single-photon detection in a strong and not-uniform magnetic field, a compact readout electronics to fit into the ePIC envelope and the use of two radiators to extend the momentum reach. The remaining effort is substantial, but is connected to more consolidated technologies, with possibly the only exception of the gas separation system for the peculiar C_2F_6 gas.

Environmental, Safety and Health (ES&H) aspects and Quality Assessment (QA planning:
Standard slow-control and interlock procedures will be implemented to control power and cooling while monitoring gas flow, humidity and temperature. The cooling system is complemented by a buffer tank to allow air flow and heat removal from the detector boxes in case of a failure of the recirculating system. Annealing of SiPM will be performed during technical stops and/or during the annual stops of the EIC machine. All the dRICH front-end electronics (FEE) will not be powered, with the exception of a few components needed to monitor and control the annealing operations. An interlock-based sistem will inhibit the FEE power-supply units during annealing. The circulating thermostat system used to cool the SiPMs will be switched to heating mode to reach a temperature of up to T = 100°C. A slow heating ramp of < 1 °C/minute will be employed to reduce thermal stress on the system. The dRICH photodetector boxes will be thermally insulated as much as possible to reduce heat leaks into neighbouring detectors while performing annealing. It is expected that the inner volume of the detector box can reach a temperature of T $\lesssim$ 100°C and will be monitored with temperature sensors. Temperature sensors will be placed on the outside of the photodetector boxes to monitor the external environment. Only a fraction of the dRICH SiPMs will perform annealing at a given time, to limit the total amount of power needs to about 20-40 kW. This is a similar to the total power consumption of the FEE during normal operations and the same safety procedures apply. Annealing power will be distributed evenly across the dRICH SiPM. In case of a power outage, the annealing current will be promptly removed from the SiPMs and their temperature will promptly drop to the temperature of the thermostat. The latter will eventually slowly cool down.
The gas volume is maintained at +1 mbar with respect the atmospheric pressure on the top, with a consequent +5 mbar overpressure defined by the hydrostatic pressure of the radiator gas on the bottom, by means of pressure regulators connected to an UPS station and a two-way bubbler. Hexafluoroethane is non-flammable and it has limited toxicity, when below 1000 ppm level and for short exposure time [**?**]. In case of a major damage of the supply pipeline or of the vessel itself, 12 m^3 of hexafluoroethane at atmospheric pressure from the vessel (0.02% of the hall volume) will mix with the air present in the experimental hall, requiring the implementation of standard ODH procedures. Hexafluoroethane has a high Global Warming Potential (GWP): 12400 for a horizon time of 100 years [92] and it is, therefore, included in the group of GreenHouse Gasses (GHG). Environment protection imposes that GHGes are not released in the atmosphere. This is obtained by using them in closed circuits, where leakages are minimized, and by collecting and sending for disposal the fraction of gas purged during circuit filling and gas recovery at the beginning and at the end of an operation period, respectively. Both closed circuit gas circulation and purged gas trapping are characterizing elements of the dRICH radiator gas system design. The maximum expected leakage rate during operation is about 20 m^3 / year assuming six-month operation.
Experience in quality assurance protocols has being gained in parallel with the R&D activity. For each critical component two stations are being organized to provide essential QA and redundancy, with a (third) station able to supports in-deep characterization on samples and serve as backup, see Table 8.32. The QA activity will be supported by workforce from all the dRICH groups. Es-

Component	QA station 1	QA station 2	QA detail and backup
Aerogel	Temple U.	BNL	INFN-BA
Gas	BNL		INFN-TS
Mirror	JLab	Duke U.	
Sensor (SiPM)	INFN CS-SA-CT	INFN-TS	INFN-BO
Readout	INFN-BO	INFN-FE	INFN-TO

Table 8.32: Planned quality assurance (QA) stations, organized in order to provide redundancy and support specific characterization studies.

sential QA parameters will be measured: integrity, refraction index, transparency, dimensions, and planarity of the aerogel; leak rate of the gas system (after completion); refractive index and transparency of the radiator gas (with the monitoring equipment of the gas system); dark count rate and PDE for the sensors; electrical connections, bias levels and data rate for the readout; dimensions, weight, reflectivity and D0 (point-like source image brigthness) for the mirrors.

Construction and assembly planning:
The construction and assembling plan assumes to compress all the necessary tasks in a short time period in between the presently known EIC milestones: start with CD3 (at the beginning of 2026) and completion 6 months in advance of installation (in October 2030). This results in an aggressive schedule in terms of workforce and funding profile. The 6 months contingency time before installation will be used to perform functionality tests, and complete the services in the experimental hall at IP6. The assembling of 1248 PDUs comprising SiPM sensors and cooling, front-end electronics and RDOs, and their integration with the services inside six detector boxes will be staged over 2 years (mainly 2027 and 2028) by the dRICH DSC in Italy. This organized effort requires a timely procurement, starting with the ALCOR chip (wafer and packaging) followed by sensors, readout electronics, and box mechanics. Cooling infrastructure and DAQ system are expected to run in parallel to the detector box construction and be mainly covered by the EIC Project. First articles of DAQ, power supply and slow control could be used for the initial functionality tests of each single detector box, but the main effort on such services is concentrated on a later stage of the plan during assembling at BNL. The detector boxes will be completed in time to be shipped to BNL and mounted on the dRICH in the second half of 2029. The dRICH vessel construction, a joint venture of the dRICH DSC and the EIC Project, will start in 2028 in order to be ready for detector assembling mid 2029. Mirror production is expected to take 2 years and is staged as soon as possible, subject to the funding profile of the EIC Project, to reduce the sole source risk. The engineering of the aerogel production is expected to extend beyond the TDR, with the consequent production led by the dRICH DSC not happening before 2027 and lasting for at least 2.5 years. An early procurement of the C_2F_6 gas by the EIC Project is planned in order to reduce the risk of a market price increase. The basic design of the radiator gas system will be completed by the end of 2026 by the dRICH DSC. The executive drawings and the system realization by the EIC Project engineering team supported by adequate technical personnel is expected during years 2027 and 2028. The layout finalization and validation of the monitoring equipment will be completed by the end of 2026, whit its realization by the dRICH DSC planned by the end of 2027. This equipment will be interfaced with the gas system in 2028, via synergistic effort between the EIC Project engineering team and the dRICH DSC. This combined group will perform the QA assessment of the gas system in 2029.

Collaborators and their role, resources and workforce:
INFN has agreed on a substantial in-kind contribution and the corresponding workforce has taken

corresponding responsibilities in the construction within the DSC. The INFN in-kind will cover the design, production and quality assurance cost of the SiPM sensors, of front-end ASIC (ALCOR), of the front-end board (FEB), of the readout boards (RDO) as well as the assembly of the above components in a compact Photo Detector Unit (PDU), including the cooling circuitry and related mechanics. It will cover the cost of the realization of the six detector boxes (containing the 208 PDUs of each sector) with the control panels and the electronic services attached (for HV/LV/daq links routing). It will contribute to the design and realization of the main vessel, the design/supervision of the powering and monitoring systems, the dRICH tagging system and data filtering in streaming mode, see Sec. 8.3.10 , and to the definition of specifications and quality assurance (QA) of all the other components and services (i.e. gas, power and cooling plants). The availability of the essential local resources as mechanical and electronic workshops and laboratory space have been negotiated. **INFN-FE** (IT): is coordinating the DSC activity and is leading the mechanical design. The group will lead the design and production of the vessel in collaboration with the EIC Project and will take care of the realization of the detector boxes and corresponding control panels for the 6 sectors. The assembly of the detector boxes is expected to happen in its laboratories. **INFN-BO** (IT): the group is leading the activity on photosensors (SiPM) and data-acquisition. It will be responsible of the procurement of SiPM, design and production the readout boards (RDO), and coordinate the integration of the various elements of the PDU. The PDU will be assembled at INFN-BO and tested/validated before being moved to INFN-FE for the installation in the detector boxes. **INFN-BA** (IT): the group is leading the aerogel activity. It will coordinate the mass production and the quality assurance (expected to be operated in the US at Temple University and BNL). **INFN-CS-SA-CT** (IT): this cluster of units will work on the QA of SiPM and front-end boards prior of the PDU assembling. They will equip test stations in SA and CS for this purpose. **INFN-GE** (IT): is carrying out a feasibility study (and if successful, the realization) of a dRICH tagger to filter the SiPM data stream. **INFN-LNS** (IT): the group will contribute to the mechanical design effort. **INFN-RM1/RM-TV** (IT): the RM1 group (and one staff person of RM-TV) has extensive experience with AI algorithms running on FPGA. They will develop algorithms for pattern recognition and data reduction on FELIX cards and the interface with the signals received by the dRICH tagger or from ePIC via GTU. **INFN-TO** (IT): the group is leading on the design, test and production of the front-end ASIC ALCOR. The group will produce the chips and the front-end cards (FEB) mounting the ALCOR, and coordinate the quality assurance tests of the chip and FEB. **INFN-TS** (IT): the group is leading the radiator gas activity and the software-simulation activity. It will lead the design of the gas system and develop a continuous monitor system (critical to maintain a good chromaticity). It will also develop a test station of SiPM (with smaller capacity with respect to the CS-SA-CT cluster). **DUKE U.** (US) is leading the mirror activity. It will coordinate the mirror production, expected to happen in the States, the corresponding QA activity, and the coating process that possibly will be realized at Stony Brook. **Jefferson Lab** (US) is contributing to the mechanical design and developing tools for mirror characterization. **Brookhaven Lab** (US) is contributing to the mechanical design and integration study. It will lead the infrastructure (installation tools, services, safety control) realization with its design authority and technical resources. **Stony Brook** (US) is developing mirror coating capability. **Temple U.** (US) is developing an aergel quality assurance facility. **M.S.Ramaiah U.** (India) is contributing to the simulation and performance study. **NISER** (India) is contributing to the performance study. **Haryana and Karnataka U.** (India) have started contrinuting to the performance study. Secondments of personnel from all the DSC groups will be organized to support the QA activity in US and the assembling phase at BNL. The EIC Project is expected to cover the procurement effort that can be more efficiently based on US, and all the safety, infrastructural and integration aspect that require specific engineering background. This include the cost of the gas, of the mirrors, of the installation tools, of the power-supply systems , of the cooling plant and the gas plant, and of the FELIX cards receiving the data from the RDO.

Institution	Nation	Main Activity
INFN-FE	Italy	Mechanics, detecor box and control panels
INFN-BO	Italy	Photosensors, photodetection unit PDU and readout board RDO
INFN-TO	Italy	ALCOR and front-end board FEB
INFN-BA	Italy	Aerogel radiator
INFN-CS-SA-CT	Italy	SiPM quality assurance
INFN-GE	Italy	dRICH tagger
INFN-LNS	Italy	Mechanical design
INFN-RM1-RM-TV	Italy	Online data reduction
INFN-TS	Italy	Radiator gas, gas system and software, SiPM quality assurance
DUKE-U,	USA	Mirror
JLab	USA	Mechanical design and mirror characterization
BNL	USA	Mechanical design, integration, infrastructure
Temple U.	USA	Aeorgel quality assurance
M.S. Ramaiah U.	India	Simulations and performance study
NISER	India	Performance study
Central U. of Haryana U.	India	Performance study
Central U. of Karnataka U.	India	Performance study

Table 8.33: Overview of Institutes and roles in the dRICH activity.

Risks and mitigation strategy:
The major risk of the dRICH gas radiator is the banning of the hexafluoroethane or more severe restriction on its usage, that can also result in increased cost or difficult procurement. The only alternative option to preserve the dRICH performance would be an eco-friendly gas with very similar refractive index, an option not available in nature at atmospheric pressure. Argon at ≈ 3 bar absolute pressure mimics with great accuracy the hexafluoroethane characteristics. It is also non-expensive, non-toxic and non-flammable. R&D is being performed within the EIC generic R&D program to establish the validity of this approach as risk mitigation strategy. Radiation damage reduces the lifetime of the SiPM as good photodetector for the dRICH performance. Estimates of the radiation level on the dRICH photodetectors are expected to be accurate. The DCR model shown in Figure 8.100 (right) is for the sensors experiencing the largest radiation levels (closer to the beam line) and for detector operation at V_{over} = 4 V and T = -30°C. Operation at lower V_{over} = 3 V and/or lower temperature T = -40°C would reduce the DCR without loss in performance, hence allowing one to accommodate larger integrated radiation levels (up to a factor 2-3) than those reported in the figure. The addition of small thermoelectric cooling (TEC) modules will be evaluated as a potential approach to boost the cooling performance, allowing one to reach an even lower operation temperature of T = -50°C and avoid possible dishomogeneities. Current R&D on new SiPM technologies for improved performance and radiation hardness are being followed up as a risk mitigation strategy and as a potential upgrade for the dRICH photodetector in the late 2030's or in the early 2040's. For two components, optical aerogel and carbon-fiber mirror, there is only one known supplier able to deliver the wanted specifications at the present stage. An early procurement should limit the risk of a market discontinuity. Within the ePIC RICH Consortium, the recently initiated R&D on mirrors at Purdue University are being followed up as potential sources of risk mitigation in the long term period, if the adaptation to the dRICH needs will be proven feasible. DSC members are part of the recent DRD4 initiative, that aims to create a worldwide collaborative environment to foster new technological breakthroughs in Cherenkov particle identification and photon detectors. Within DRD4, there are many development areas of interest for the dRICH program, in particular gasses or mixtures alternative to the greenhouse fluorocarbon gasses and radiation hard SiPM.

References

[1] A. Bacchetta, V. Bertone, C. Bissolotti, G. Bozzi, M. Cerutti, F. Delcarro, M. Radici, L. Rossi, and A. Signori, "Flavor dependence of unpolarized quark transverse momentum distributions from a global fit," *JHEP*, vol. 08, p. 232, 2024.

[2] Irene Dutta and Christopher Madrid and Ryan Heller and Shirsendu Nanda and Danush Shekar and Claudio San Martín and Matías Barría and Artur Apresyan and Zhenyu Ye and William K. Brooks and Wei Chen and Gabriele D'Amen and Gabriele Giacomini and Alessandro Tricoli and Aram Hayrapetyan and Hakseong Lee and Ohannes Kamer Köseyan and Sergey Los and Koji Nakamura and Sayuka Kita and Tomoka Imamura and Cristían Peña and Si Xie, "Results for pixel and strip centimeter-scale AC-LGAD sensors with a 120 GeV proton beam," 7 2024.

[3] M. Tabata *et al.*, "Silica aerogel radiator for use in the A-RICH system utilized in the Belle II experiment," *Nucl. Instrum. Meth. A*, vol. 766, pp. 212–216, 2014.

[4] R. Brun and F. Rademakers, "ROOT: An object oriented data analysis framework," *Nucl. Instrum. Meth. A*, vol. 389, pp. 81–86, 1997.

[5] J. de Favereau, C. Delaere, P. Demin, A. Giammanco, V. Lemaître, A. Mertens, and M. Selvaggi, "Delphes 3: a modular framework for fast simulation of a generic collider experiment," *Journal of High Energy Physics*, vol. 2014, Feb. 2014.

[6] F. T. Acosta, B. Karki, P. Karande, A. Angerami, M. Arratia, K. Barish, R. Milton, S. Morán, B. Nachman, and A. Sinha, "The optimal use of segmentation for sampling calorimeters," *JINST*, vol. 19, no. 06, p. P06002, 2024.

[7] M. M. David Ruth, Alex Jentsch, "Advanced methods for roman pots reconstruction at the eic." https://indico.cern.ch/event/1199314/contributions/5193191/attachments/2619028/4527696/DIS_RNDtalk_DRuth.pdf, 2023.

[8] M. Tabata, I. Adachi, H. Kawai, T. Sumiyoshi, and H. Yokogawa, "Hydrophobic silica aerogel production at kek," *Nuclear Instruments and Methods in Physics Research Section A: Accelerators, Spectrometers, Detectors and Associated Equipment*, vol. 668, pp. 64–70, 2012.

[9] R. Abdul Khalek *et al.*, "Science Requirements and Detector Concepts for the Electron-Ion Collider: EIC Yellow Report," *Nucl. Phys. A*, vol. 1026, p. 122447, 2022.

[10] A. Accardi *et al.*, "Electron Ion Collider: The Next QCD Frontier: Understanding the glue that binds us all," *Eur. Phys. J. A*, vol. 52, no. 9, p. 268, 2016.

[11] A. Accardi *et al.*, "Electron Ion Collider: The Next QCD Frontier: Understanding the glue that binds us all," *Eur. Phys. J. A*, vol. 52, no. 9, p. 268, 2016.

[12] "National Academies of Sciences, Engineering, and Medicine, An Assessment of U.S.-Based Electron-Ion Collider Science," *The National Academies Press,Washington, DC*, 2018.

[13] J. K. Adkins *et al.*, "Design of the ECCE Detector for the Electron Ion Collider," 9 2022.

[14] J. Adam *et al.*, "ATHENA detector proposal — a totally hermetic electron nucleus apparatus proposed for IP6 at the Electron-Ion Collider," *JINST*, vol. 17, no. 10, p. P10019, 2022.

[15] M. Arratia, D. Britzger, O. Long, and B. Nachman, "Reconstructing the kinematics of deep inelastic scattering with deep learning," *Nucl. Instrum. Meth. A*, vol. 1025, p. 166164, 2022.

[16] A. MetZhao:2016rfuz and A. Vossen, "Parton Fragmentation Functions," *Prog. Part. Nucl. Phys.*, vol. 91, pp. 136–202, 2016.

[17] P. J. Mulders and R. D. Tangerman, "The Complete tree level result up to order 1/Q for polarized deep inelastic leptoproduction," *Nucl. Phys. B*, vol. 461, pp. 197–237, 1996. [Erratum: Nucl.Phys.B 484, 538–540 (1997)].

[18] A. Bacchetta, M. Diehl, K. Goeke, A. Metz, P. J. Mulders, and M. Schlegel, "Semi-inclusive deep inelastic scattering at small transverse momentum," *JHEP*, vol. 02, p. 093, 2007.

[19] D. W. Sivers, "Single Spin Production Asymmetries from the Hard Scattering of Point-Like Constituents," *Phys. Rev. D*, vol. 41, p. 83, 1990.

[20] D. W. Sivers, "Hard scattering scaling laws for single spin production asymmetries," *Phys. Rev. D*, vol. 43, pp. 261–263, 1991.

[21] E. C. Aschenauer, V. Batozskaya, S. Fazio, K. Gates, H. Moutarde, D. Sokhan, H. Spiesberger, P. Sznajder, and K. Tezgin, "EpIC: novel Monte Carlo generator for exclusive processes," *Eur. Phys. J. C*, vol. 82, no. 9, p. 819, 2022.

[22] D. Boer *et al.*, "Physics case for quarkonium studies at the Electron Ion Collider," 9 2024.

[23] L. Frankfurt, M. Strikman, and M. Zhalov, "Elastic and large t rapidity gap vector meson production in ultraperipheral proton–ion collisions," *Physics Letters B*, vol. 640, no. 4, pp. 162–169, 2006.

[24] A. Tumasyan, W. Adam, and Others, "Probing small bjorken-x nuclear gluonic structure via coherent j/ψ photoproduction in ultraperipheral pb-pb collisions at $\sqrt{s_{\mathrm{NN}}} = 5.02$ TeV," *Phys. Rev. Lett.*, vol. 131, p. 262301, Dec 2023.

[25] A. Baltz, G. Baur, D. d'Enterria, L. Frankfurt, F. Gelis, V. Guzey, K. Hencken, Y. Kharlov, M. Klasen, S. Klein, V. Nikulin, J. Nystrand, I. Pshenichnov, S. Sadovsky, E. Scapparone, J. Seger, M. Strikman, M. Tverskoy, R. Vogt, S. White, U. Wiedemann, P. Yepes, and M. Zhalov, "The physics of ultraperipheral collisions at the lhc," *Physics Reports*, vol. 458, no. 1, pp. 1–171, 2008.

[26] J.-P. Lansberg, K. Lynch, C. Van Hulse, and R. McNulty, "Inclusive photoproduction of vector quarkonium in ultra-peripheral collisions at the LHC," 9 2024.

[27] S. R. Klein and H. Mäntysaari, "Imaging the nucleus with high-energy photons," *Nature Rev. Phys.*, vol. 1, no. 11, pp. 662–674, 2019.

[28] K. J. Eskola, C. A. Flett, V. Guzey, T. Löytäinen, and H. Paukkunen, "Exclusive quarkonium photoproduction in A+A UPCs at the LHC in NLO pQCD," *PoS*, vol. HardProbes2023, p. 107, 2024.

[29] C. A. Flett, J. P. Lansberg, S. Nabeebaccus, M. Nefedov, P. Sznajder, and J. Wagner, "Exclusive vector-quarkonium photoproduction at NLO in alpha_s in collinear factorisation with evolution of the generalised parton distributions and high-energy resummation," 9 2024.

[30] S. R. Klein, J. Nystrand, J. Seger, Y. Gorbunov, and J. Butterworth, "Starlight: A monte carlo simulation program for ultra-peripheral collisions of relativistic ions," *Computer Physics Communications*, vol. 212, pp. 258–268, 2017.

[31] Y. X. Zhao, A. Deshpande, J. Huang, K. S. Kumar, and S. Riordan, "Neutral-Current Weak Interactions at an EIC," *Eur. Phys. J. A*, vol. 53, no. 3, p. 55, 2017.

[32] "Radiation Doses." https://wiki.bnl.gov/EPIC/index.php?title=Radiation_Doses.

[33] S. Agostinelli *et al.*, "GEANT4—a simulation toolkit," *Nucl. Instrum. Meth. A*, vol. 506, p. 250, 2003.

[34] "The electron-ion collider user group.".

[35] R. A. Khalek *et al.*, "Science Requirements and Detector Concepts for the Electron-Ion Collider: EIC Yellow Report," *Nucl. Instr. and Meth. A*, vol. 1026, p. 122447, 2022.

[36] "The epic collaboration website.".

[37] A. Collaboration, "Technical Design report for the ALICE Inner Tracking System 3 - ITS3 ; A bent wafer-scale monolithic pixel detector," tech. rep., CERN, Geneva, 2024.

[38] M. Karagounis, D. Arutinov, M. Barbero, F. Huegging, H. Krueger, and N. Wermes, "An integrated shunt-ldo regulator for serial powered systems," in *2009 Proceedings of ESSCIRC*, pp. 276–279, 2009.

[39] A. Paramonov, "FELIX: the Detector Interface for the ATLAS Experiment at CERN," *EPJ Web Conf.*, vol. 251, p. 04006, 2021.

[40] lpGBT Design Team, "lpgbt documentation – release," 2024.

[41] J. Troska *et al.*, "The VTRx+, an optical link module for data transmission at HL-LHC," 2017.

[42] D. Higinbotham and et *al*., "Science requirements and detector concepts for the electron-ion collider: Eic yellow report," *Nuclear Physics A*, vol. 1026, p. 122447, 2022.

[43] F. Willeke and J. Beebe-Wang, "Electron ion collider conceptual design report 2021," 2 2021.

[44] ePIC, "Summary of epic background rates," 2024.

[45] EIC, "Eic detector geometry," 2024.

[46] D. Neyret, P. Abbon, M. Anfreville, V. Andrieux, Y. Bedfer, D. Durand, S. Herlant, N. d'Hose, F. Kunne, S. Platchkov, F. Thibaud, M. Usseglio, and M. Vandenbroucke, "Aging effects in the compass hybrid gem-micromegas pixelized detectors," *Nuclear Instruments and Methods in Physics Research Section A: Accelerators, Spectrometers, Detectors and Associated Equipment*, vol. 1065, p. 169511, 2024.

[47] C. Altunbas, M. Capeans, K. Dehmelt, J. Ehlers, J. Friedrich, I. Konorov, A. Gandi, S. Kappler, B. Ketzer, R. De Oliveira, S. Paul, A. Placci, L. Ropelewski, F. Sauli, F. Simon, and M. van Stenis, "Construction, test and commissioning of the triple-gem tracking detector for compass," *Nuclear Instruments and Methods in Physics Research Section A: Accelerators, Spectrometers, Detectors and Associated Equipment*, vol. 490, no. 1, pp. 177–203, 2002.

[48] T. Kawamoto *et al.*, "New Small Wheel Technical Design Report," *CERN-LHCC-2013-006, ATLAS-TDR-020, CERN-LHCC-2013-006, ATLAS-TDR-020*, 6 2013.

[49] M. Poli Lener, G. Bencivenni, R. de Olivera, G. Felici, S. Franchino, M. Gatta, M. Maggi, G. Morello, and A. Sharma, "The μ-rwell: A compact, spark protected, single amplification-stage mpgd," *Nuclear Instruments and Methods in Physics Research Section A: Accelerators, Spectrometers, Detectors and Associated Equipment*, vol. 824, pp. 565–568, 2016. Frontier Detectors for Frontier Physics: Proceedings of the 13th Pisa Meeting on Advanced Detectors.

[50] E. Farina, B. A. Gonzalez, P. Iengo, L. Longo, J. Samarati, G. Sekhniaidze, O. Sidiropoulou, and J. Wotschack, "Resistive micromegas high-rate and long-term ageing studies at the cern gamma irradiation facility," *Nuclear Instruments and Methods in Physics Research Section A: Accelerators, Spectrometers, Detectors and Associated Equipment*, vol. 1042, p. 167423, 2022.

[51] M. Chefdeville and et *al.*, "Development of micromegas detectors with resistive anode pads," *Nuclear Instruments and Methods in Physics Research Section A: Accelerators, Spectrometers, Detectors and Associated Equipment*, vol. 1003, p. 165268, 2021.

[52] L. Shekhtman, G. Fedotovich, A. Kozyrev, V. Kudryavtsev, T. Maltsev, and A. Ruban, "Development of μrwell detectors for the upgrade of the tracking system of cmd-3 detector," *Nuclear Instruments and Methods in Physics Research Section A: Accelerators, Spectrometers, Detectors and Associated Equipment*, vol. 936, pp. 401–404, 2019.

[53] A. Acker, D. Attié, S. Aune, J. Ball, P. Baron, Q. Bertrand, D. Besin, T. Bey, F. Bossù, R. Boudouin, M. Boyer, G. Christiaens, P. Contrepois, M. Defurne, E. Delagnes, M. Garçon, F. Georges, J. Giraud, R. Granelli, N. Grouas, C. Lahonde-Hamdoun, T. Lerch, I. Mandjavidze, O. Meunier, Y. Moudden, S. Procureur, M. Riallot, F. Sabatié, M. Vandenbroucke, and E. Virique, "The clas12 micromegas vertex tracker," *Nuclear Instruments and Methods in Physics Research Section A: Accelerators, Spectrometers, Detectors and Associated Equipment*, vol. 957, p. 163423, 2020.

[54] I. Giomataris, R. De Oliveira, S. Andriamonje, S. Aune, G. Charpak, P. Colas, A. Giganon, P. Rebourgeard, and P. Salin, "Micromegas in a bulk," *Nucl. Instrum. Meth. A*, vol. 560, pp. 405–408, 2006.

[55] H. Schindler and R. Veenhof, "Garfield++," 2024.

[56] K. Gnanvo and et *al.*, "Development of double-sided thin-gap gem-μrwell for tracking at the eic." https://www.jlab.org/sites/default/files/eic_rd_prgm/files/2023_Proposals/20230714_eRD_tgMPGD_Proposal_FY23_Final_EICGENRandD2023_16.pdf, 2023.

[57] K. Gnanvo, N. Liyanage, B. Mehl, and R. de Oliveira, "Performance of a resistive micro-well detector with capacitive-sharing strip anode readout," *Nuclear Instruments and Methods in Physics Research Section A: Accelerators, Spectrometers, Detectors and Associated Equipment*, vol. 1047, p. 167782, 2023.

[58] M. Calvi, P. Carniti, C. Gotti, C. Matteuzzi, and G. Pessina, "Single photon detection with SiPMs irradiated up to 10^{14} cm^{-2} 1-MeV-equivalent neutron fluence," *Nucl. Instrum. Meth. A*, vol. 922, pp. 243–249, 2019.

[59] "Technical Design Report: A High-Granularity Timing Detector for the ATLAS Phase-II Upgrade," tech. rep., CERN, Geneva, 2020.

[60] C. Madrid, R. Heller, C. San Martín, S. Nanda, A. Apresyan, W. Brooks, W. Chen, G. Giacomini, O. Kamer Köseyan, S. Los, C. Peña, R. Rios, A. Tricoli, S. Xie, and Z. Ye, "First survey of centimeter-scale ac-lgad strip sensors with a 120 gev proton beam," *Journal of Instrumentation*, vol. 18, p. P06013, June 2023.

[61] C. Bishop, A. Das, J. Ding, M. Gignac, F. Martinez-McKinney, S. Mazza, A. Molnar, N. Nagel, M. Nizam, J. Ott, H.-W. Sadrozinski, B. Schumm, A. Seiden, T. Shin, A. Summerell, M. Wilder, and Y. Zhao, "Long-distance signal propagation in ac-lgad," *Nuclear Instruments and Methods in Physics Research Section A: Accelerators, Spectrometers, Detectors and Associated Equipment*, vol. 1064, p. 169478, 2024.

[62] L. Menzio *et al.*, "First test beam measurement of the 4D resolution of an RSD pixel matrix connected to a FAST2 ASIC," *Nucl. Instrum. Meth. A*, vol. 1065, p. 169526, 2024.

[63] S. Xie, A. Apresyan, R. Heller, C. Madrid, I. Dutta, A. Hayrapetyan, S. Los, C. Peña, and T. Zimmerman, "Design and performance of the fermilab constant fraction discriminator asic," *Nuclear Instruments and Methods in Physics Research Section A: Accelerators, Spectrometers, Detectors and Associated Equipment*, vol. 1056, p. 168655, 2023.

[64] J. D. Brandenburg *et al.*, "The STAR Forward Silicon Tracker," 7 2024.

[65] C. Chock, K. Flood, L. Macchiarulo, F. Martinez-Mckinney, A. Martinez-Rojas, S. Mazza, I. Mostafanezhad, M. Nizam, J. Ott, R. Perron, E. Ryan, H.-W. Sadrozinski, B. Schumm, A. Seiden, K. Shin, M. Tarka, D. Uehara, M. Wilder, and Y. Zhao, "First test results of the transimpedance amplifier stage of the ultra-fast hpsoc asic," *Journal of Instrumentation*, vol. 18, p. C02016, feb 2023.

[66] O. H. W. Siegmund *et al.*, "Advances in microchannel plates and photocathodes for ultraviolet photon counting detectors," *Society of Photo-Optical Instrumentation Engineers Proceedings*, vol. 81450J.

[67] C. J. Hamel *et al.*, "LAPPD and HRPPD: Upcoming Upgrades to Incom's Fast Photosensors,"

[68] "Popecki." https://indico.cfnssbu.physics.sunysb.edu/event/265/contributions/922/attachments/261/411/LAPPD%20and%20HRPPD%20update%20EIC%20Workshop%2005-08-2024.pptx.

[69] J. A. et al, "Performance of an LAPPD in magnetic fields," *Nucl.Instrum.Meth. A*, no. 1072, p. 170122, 2025.

[70] "EICROC ASIC." https://indico.bnl.gov/event/18539/contributions/73731/attachments/46348/78403/CdLT_EICROC_6mar23.pdf.

[71] "Organization for Micro-Electronics desiGn and Applications." https://portail.polytechnique.edu/omega/.

[72] J. Anderson *et al.*, "FELIX: a PCIe based high-throughput approach for interfacing front-end and trigger electronics in the ATLAS Upgrade framework," *JINST*, vol. 11, no. 12, p. C12023, 2016.

[73] "Chiba Aerogel Factory Co., Ltd.." https://www.aerogel-factory.jp/.

[74] M. Yonenaga *et al.*, "Performance evaluation of the aerogel RICH counter for the Belle II spectrometer using early beam collision data," *Prog. Theor. Exp. Phys.*, no. 093H01, 2020.

[75] "ePIC IRT Package." https://github.com/eic/irt/tree/pfrich.

[76] R. Brun and F. Rademakers, "ROOT - An Object Oriented Data Analysis Framework, Proceedings AIHENP'96 Workshop, Lausanne," *Nucl. Inst. & Meth. in Phys. Res. A*, no. 389, pp. 81–86, 1997.

[77] M. Tabata, I. Adachi, Y. Hatakeyama, H. Kawai, T. Morita, and T. Sumiyoshi, "Large-area silica aerogel for use as cherenkov radiators with high refractive index, developed by supercritical carbon dioxide drying," *The Journal of Supercritical Fluids*, vol. 110, pp. 183–192, 2016.

[78] "CAEN A1515BV 16-channel floating ground High Voltage module." https://www.caen.it/products/a1515b/.

[79] "CAEN SY4527 High Voltage mainframe." https://www.caen.it/products/SY4527/.

[80] "Wiener Mpod Low Voltage system." https://www.wiener-d.com/power-supplies/mpod-lv-hv/.

[81] A. Buzykaev, A. Danilyuk, S. Ganzhur, E. Kravchenko, and A. Onuchin, "Measurement of optical parameters of aerogel," *Nuclear Instruments and Methods in Physics Research Section A: Accelerators, Spectrometers, Detectors and Associated Equipment*, vol. 433, no. 1, pp. 396–400, 1999.

[82] A. J. Hunt, "Light scattering for aerogel characterization," *Journal of Non-Crystalline Solids*, vol. 225, pp. 303–306, 1998.

[83] S. K. Sahu *et al.*, "Measurement of Radiation Damage on Silica Aerogel Cherenkov Radiator," *Nucl. Instrum. Meth. A*, vol. 382, pp. 441–446, 1996.

[84] R. Abjean, A. Bideau-Mehu, and Y. Guern, "Refractive index of hexafluoroethane (C-2F-6) in the 300-nm to 150-nm wavelength range," *Nucl. Instrum. Meth. A*, vol. 354, pp. 417–418, 1995.

[85] C. Piemonte and A. Gola, "Overview on the main parameters and technology of modern Silicon Photomultipliers," *Nucl. Instrum. Meth. A*, vol. 926, pp. 2–15, 2019.

[86] L. P. Rignanese, P. Antonioli, R. Preghenella, and E. Scapparone, "SiPMs and examples of applications for low light detection in particle and astroparticle physics," *Riv. Nuovo Cim.*, vol. 47, no. 5, pp. 299–349, 2024. [Erratum: Riv.Nuovo Cim. 47, (2024)].

[87] S. España, L. Fraile, J. Herraiz, J. Udías, M. Desco, and J. Vaquero, "Performance evaluation of sipm photodetectors for pet imaging in the presence of magnetic fields," *Nuclear Instruments and Methods in Physics Research Section A: Accelerators, Spectrometers, Detectors and Associated Equipment*, vol. 613, no. 2, pp. 308–316, 2010.

[88] F. Acerbi *et al.*, "Cryogenic Characterization of FBK HD Near-UV Sensitive SiPMs," *IEEE Trans. Electron. Dev.*, vol. 64, pp. 521–526, 10 2016.

[89] S. Merzi, F. Acerbi, C. Aicardi, D. Fiore, V. Goiffon, A. G. Gola, O. Marcelot, A. Materne, and O. Saint-Pe, "Radiation Damage on Silicon Photomultipliers from Ionizing and Non-Ionizing Radiation of Low-Earth Orbit Operations," *Sensors*, vol. 24, no. 15, p. 4990, 2024.

[90] E. Garutti and Y. Musienko, "Radiation damage of SiPMs," *Nucl. Instrum. Meth. A*, vol. 926, pp. 69–84, 2019.

[91] T. Tsang, T. Rao, S. Stoll, and C. Woody, "Neutron radiation damage and recovery studies of SiPMs," *JINST*, vol. 11, no. 12, p. P12002, 2016.

[92] EU, "Regulation (EU) 2024/573 of the European Parliament and of the Council on fluorinate greehouse gases," *https://eur-lex.europa.eu/eli/reg/2024/573/oj*, 2024.

[93] E. Nappi, "Aerogel and its applications to rich detectors," *Nuclear Physics B - Proceedings Supplements*, vol. 61, no. 3, pp. 270–276, 1998. Proceedings of the Fifth International Conference on Advanced Technology and Particle Physics.

[94] M. Kubantsev, I. Larin, and A. Gasparian, "Performance of the PrimEx electromagnetic calorimeter," *AIP Conf. Proc.*, vol. 867, no. 1, pp. 51–58, 2006.

[95] T. Horn *et al.*, "Scintillating crystals for the Neutral Particle Spectrometer in Hall C at JLab," *Nucl. Instrum. Meth. A*, vol. 956, p. 163375, 2020.

[96] A. Asaturyan *et al.*, "Electromagnetic calorimeters based on scintillating lead tungstate crystals for experiments at Jefferson Lab," *Nucl. Instrum. Meth. A*, vol. 1013, p. 165683, 2021.

[97] F. Ameli *et al.*, "Streaming readout for next generation electron scattering experiments," *Eur. Phys. J. Plus*, vol. 137, no. 8, p. 958, 2022.

[98] T. D. Beattie *et al.*, "Construction and Performance of the Barrel Electromagnetic Calorimeter for the GlueX Experiment," *Nucl. Instrum. Meth. A*, vol. 896, pp. 24–42, 2018.

[99] Y. Suda *et al.*, "Performance evaluation of the high-voltage CMOS active pixel sensor AstroPix for gamma-ray space telescopes," *Nucl. Instrum. Meth. A*, vol. 1068, p. 169762, 2024.

[100] ePIC Collaboration, "Background studies - epic." https://wiki.bnl.gov/EPIC/index.php?title=Background, 2023. Accessed: 2024-09-28.

[101] O. D. Tsai *et al.*, "Results of \& on a new construction technique for W/ScFi Calorimeters," *J. Phys. Conf. Ser.*, vol. 404, p. 012023, 2012.

[102] C. A. Aidala *et al.*, "Design and Beam Test Results for the sPHENIX Electromagnetic and Hadronic Calorimeter Prototypes," *IEEE Trans. Nucl. Sci.*, vol. 65, no. 12, pp. 2901–2919, 2018.

[103] T. Nicholls *et al.*, "Performance of an electromagnetic lead / scintillating fiber calorimeter for the H1 detector," *Nucl. Instrum. Meth. A*, vol. 374, pp. 149–156, 1996.

[104] O. D. Tsai *et al.*, "Development of a forward calorimeter system for the STAR experiment," *J. Phys. Conf. Ser.*, vol. 587, no. 1, p. 012053, 2015.

[105] F. Aaron *et al.*, "Measurement of the proton structure function fl(x,q2) at low x," *Physics Letters B*, vol. 665, no. 4, pp. 139–146, 2008.

[106] R.-D. Appuhn *et al.*, "The h1 lead/scintillating-fibre calorimeter," *Nuclear Instruments and Methods in Physics Research Section A: Accelerators, Spectrometers, Detectors and Associated Equipment*, vol. 386, no. 2, pp. 397–408, 1997.

[107] "SiPM radiation hardness study." https://indico.bnl.gov/event/24087/#17-further-rad-hard-studies-an.

[108] A. White *et al.*, "Design, construction and commissioning of a technological prototype of a highly granular sipm-on-tile scintillator-steel hadronic calorimeter," *Journal of Instrumentation*, vol. 18, p. P11018, nov 2023.

[109] V. Andrieux, R. Nothnagel, C. Riedl, and D. Sharma, "Vector-meson reconstruction in the epic backward hcal," tech. rep., UIUC, nov 2024. https://doi.org/10.5281/zenodo.14200156.

[110] M. Salajegheh, H. Khanpour, U.-G. Meißner, H. Hashamipour, and M. Soleymaninia, "Determination of diffractive PDFs from a global QCD analysis of inclusive diffractive DIS and dijet cross-section measurements at HERA," *Phys. Rev. D*, vol. 107, no. 9, p. 094038, 2023.

[111] E. Meschi, T. Monteiro, C. Seez, and P. Vikas, "Electron Reconstruction in the CMS Electromagnetic Calorimeter," tech. rep., CERN, Geneva, 2001.

[112] "The algorithm for the PWO calorimeter." https://www.jlab.org/primex/weekly_meetings/primexII/slides_2012_01_20/island_algorithm.pdf.

[113] A. Laudrain and on behalf of the CALICE Collaboration, "The calice ahcal: a highly granular sipm-on-tile hadron calorimeter prototype," *Journal of Physics: Conference Series*, vol. 2374, p. 012017, nov 2022.

[114] "The Phase-2 Upgrade of the CMS Endcap Calorimeter," tech. rep., CERN, Geneva, 2017.

[115] M. Arratia *et al.*, "A high-granularity calorimeter insert based on SiPM-on-tile technology at the future Electron-Ion Collider," *Nucl. Instrum. Meth. A*, vol. 1047, p. 167866, 2023.

[116] M. Arratia, B. Bagby, P. Carney, J. Huang, R. Milton, S. J. Paul, S. Preins, M. Rodriguez, and W. Zhang, "Beam Test of the First Prototype of SiPM-on-Tile Calorimeter Insert for the EIC Using 4 GeV Positrons at Jefferson Laboratory," *Instruments*, vol. 7, no. 4, p. 43, 2023.

[117] S. J. Paul and M. Arratia, "Leveraging staggered tessellation for enhanced spatial resolution in high-granularity calorimeters," *Nucl. Instrum. Meth. A*, vol. 1060, p. 169044, 2024.

[118] M. Arratia, L. Garabito Ruiz, J. Huang, S. J. Paul, S. Preins, and M. Rodriguez, "Studies of time resolution, light yield, and crosstalk using SiPM-on-tile calorimetry for the future Electron-Ion Collider," *JINST*, vol. 18, no. 05, p. P05045, 2023.

[119] R. Milton, S. J. Paul, B. Schmookler, M. Arratia, P. Karande, A. Angerami, F. T. Acosta, and B. Nachman, "Design of a SiPM-on-Tile ZDC for the future EIC and its Performance with Graph Neural Networks," 5 2024.

[120] "Point Cloud Deep Learning Methods for Pion Reconstruction in the ATLAS Experiment," tech. rep., CERN, Geneva, 2022. All figures including auxiliary figures are available at https://atlas.web.cern.ch/Atlas/GROUPS/PHYSICS/PUBNOTES/ATL-PHYS-PUB-2022-040.

[121] S. Lai *et al.*, "Software Compensation for Highly Granular Calorimeters using Machine Learning," *JINST*, vol. 19, p. P04037, 2024.

[122] ePIC Collaboration, "Far-forward detectors - epic." https://wiki.bnl.gov/EPIC/index.php?title=FarForward, 2024. Accessed: 2024-12-06.

[123] E. C. Aschenauer, S. Fazio, G. Giacomini, A. Jentsch, A. Kiselev, and A. Tricoli, "Sensors for roman pots at the eic." https://indico.bnl.gov/event/7449/contributions/35871/attachments/27124/41452/Tricoli_Roman_Pots_EIC_TempleMgt_ACLGAD_march2020.pdf, 2020.

[124] "lpGBT Documentation."

[125] G. B. et al., "HGCROC-Si and HGCROC-SiPM: the front-end readout ASICs for the CMS HGCAL," in *IEEE Nuclear Science Symposium and Medical Imaging Conference (NSS/MIC)*, pp. 1–4, 2020.

[126] X. H. et al., "The testing and performance of the ETROC2 for CMS MTD Endcap Timing Layer (ETL) upgrade," in *2024 IEEE Nuclear Science Symposium (NSS), Medical Imaging Conference (MIC) and Room Temperature Semiconductor Detector Conference (RTSD)*, pp. 1–2, 2024.

[127] S. B. et al, "SAMPA chip: a new ASIC for the ALICE TPC and MCH upgrades.," *Journal of Instrumentation*, February 2016.

[128] A. Pilyar, "The 32-channel Readout Front end Card FEC32S based on SAMPA ASIC for the Dubna NICA TPC," in *2018 IEEE XXVII International Scientific Conference Electronics – ET*, pp. 1–3, 2018.

[129] J. Troska, A. Brandon-Bravo, S. Detraz, A. Kraxner, L. Olanterä, C. Scarcella, C. Sigaud, C. Soos, and F. Vasey, "The VTRx+, an optical link module for data transmission at HL-LHC," *PoS*, vol. TWEPP-17, p. 048, 2017.

[130] J. Anderson *et al.*, "FELIX: a PCIe based high-throughput approach for interfacing front-end and trigger electronics in the ATLAS Upgrade framework," *JINST*, vol. 11, no. 12, p. C12023, 2016.

[131] R. A. et al., "APEIRON: A framework for high level programming of dataflow applications on Multi-FPGA systems," *EPJ Web of Conferences*, no. 11002, 2024.